Tectonics

Supporting Information for

Rapid Oligocene to early Miocene extension along the Grant Range detachment system, Nevada, U.S.A.: insights from multi-part cooling histories of footwall rocks

Sean P. Long[1], Matthew T. Heizler[2], Stuart N. Thomson[3], Peter W. Reiners[3], Joan E. Fryxell[4]

[1]*School of the Environment, Washington State University, Pullman, WA 99164*

[2]*New Mexico Bureau of Geology and Mineral Resources, New Mexico Tech, Socorro, NM 87801*

[3]*Department of Geosciences, University of Arizona, Tucson, AZ 85721, USA*

[4]*Department of Geological Sciences, California State University, San Bernardino, CA 92407*

Contents of this file

Introduction

Supporting information for this paper includes text, figures, and tables that give information on: the thicknesses of Grant Range rock units, geologic mapping in the western part of the southern Grant Range, oil well lithology logs, descriptions of the methodology used to estimate tilting accommodated by set 2 normal faulting, detailed descriptions of the geometries and field relations of set 1 detachment faults, methodology of mineral separation, methodology and supporting data for the $^{40}Ar/^{39}Ar$ analyses and multi-diffusion domain modeling, methodology and supporting data for fission-track and (U-Th)/He analyses, pictures and graphs demonstrating U zonation in zircons, methodology of HeFTy thermal modeling, and methodology and parameters for Midland Valley Move kinematic forward modeling.

Text S1. Thicknesses of rock units in the southern Grant Range.

Thicknesses of stratigraphic units were estimated from cross section A-A' where possible. Complete sections of several map units were not exposed, and only minimum thicknesses could be estimated. For several of these units, published thickness estimates from nearby studies in the Grant Range were used (Table S1). However, for several units, including the Cambrian Prospect Mountain Quartzite and the Cambrian Sidehill Spring Formation, complete thicknesses are not exposed anywhere in the Grant Range. For these units, minimum tectonic thicknesses estimated from the cross section are shown (Table S1).

Table S1. Data supporting thicknesses of map units in the southern Grant Range.

Unit name	Lumped unit abbreviation	Thickness constraints on A-A' (ft)	Published thickness range (ft)	Thickness used on A-A' (ft)
Oligocene (26.2 ± 0.5 Ma) Shingle Pass Tuff	Pg	≥1200	-	1200 (minimum)
Oligocene (~27.2-29.7 Ma) Needles Range Formation	Pg	750	-	750
Oligocene Forest Home Ignimbrite	Pg	200	-	200
Oligocene (31.2 ± 0.6 Ma - 32.2 ± 0.4 Ma) Windous Butte Formation	Pg	1100	-	1100
Eocene-Oligocene Currant Tuff	Pg	100-450	-	100-450
Eocene (~34.1 Ma) Stone Cabin Formation	Pg	0-350	-	0-350
Paleocene-Eocene Sheep Pass Formation	Pg	100-300	-	300
Pennsylvanian Ely Limestone	IP	≥150	800-1600 (*1, 3*)	500 (minimum)
Mississippian Chainman Shale	M	≥550	650-1400 (*3*), 1250 (*6*)	1000
Mississippian Joana Limestone	M	1150	-	1150
Devonian Guilmette Formation	D	≥600	1800-2200 (*1, 3*)	1800
Devonian Simonson Dolomite	D	≥1100	700-1000 (*1, 3, 6*)	1150 (minimum)
Devonian Sevy Dolomite	D	≥750	800 *(3)*	800
Silurian Laketown Dolomite	S	≥400	1200-1350 (*1, 2*)	1200
Ordovician Ely Springs Dolomite	O	550	-	550
Ordovician Eureka Quartzite	O	400	-	400
Ordovician Pogonip Group	O	≥2300	3800-4200 (*2, 3, 5*)	4000
Cambrian Little Meadows Formation	Cu	not exposed	100-300 (*4, 5, 6*)	300
Cambrian Sidehill Spring Formation	Cu	≥8500	4000-7000 *(4)*, 9300 *(6)*	8600 (minimum)
Cambrian Pole Canyon Limestone	Cl	≥1000	1400 (*4*)	1400
Cambrian Pioche Shale	Cl	not exposed	600-800 (*2, 4*)	800
Cambrian Prospect Mountain Quartzite	Cl	≥9100	≥3000-4500 (*3, 4*)	9100 (minimum)

Data sources:
1 - Moores et al. (1968); *2* - Cebull (1970); *3* - Hyde and Huttrer (1970); *4* - Fryxell (1988); *5* - Camilleri (2013); 6 - Long and Walker (2015)

Text S2. Geologic mapping in the western Grant Range.

In the western part of the Grant Range, cross section A-A' is supported by unpublished 1:24,000-scale geologic mapping within the Bullwhacker Springs 7.5' quadrangle performed by J. Fryxell. Figure S1 shows a simplified version of the area of this geologic map that lies along and in proximity to the cross section line. Similar unit divisions are used for Cambrian, Ordovician, and Devonian rocks as shown on Figures 2 and 3 in the text. Set 1 detachment Faults 1, 2, and 8 are labeled (note: in the eastern part of the map,

Fault 1 consists of two closely-spaced, subparallel faults that bound a <20-30 m thick sheet of intervening rock; see detailed discussion below).

Figure S1. Geologic map of the western part of the southern Grant Range.

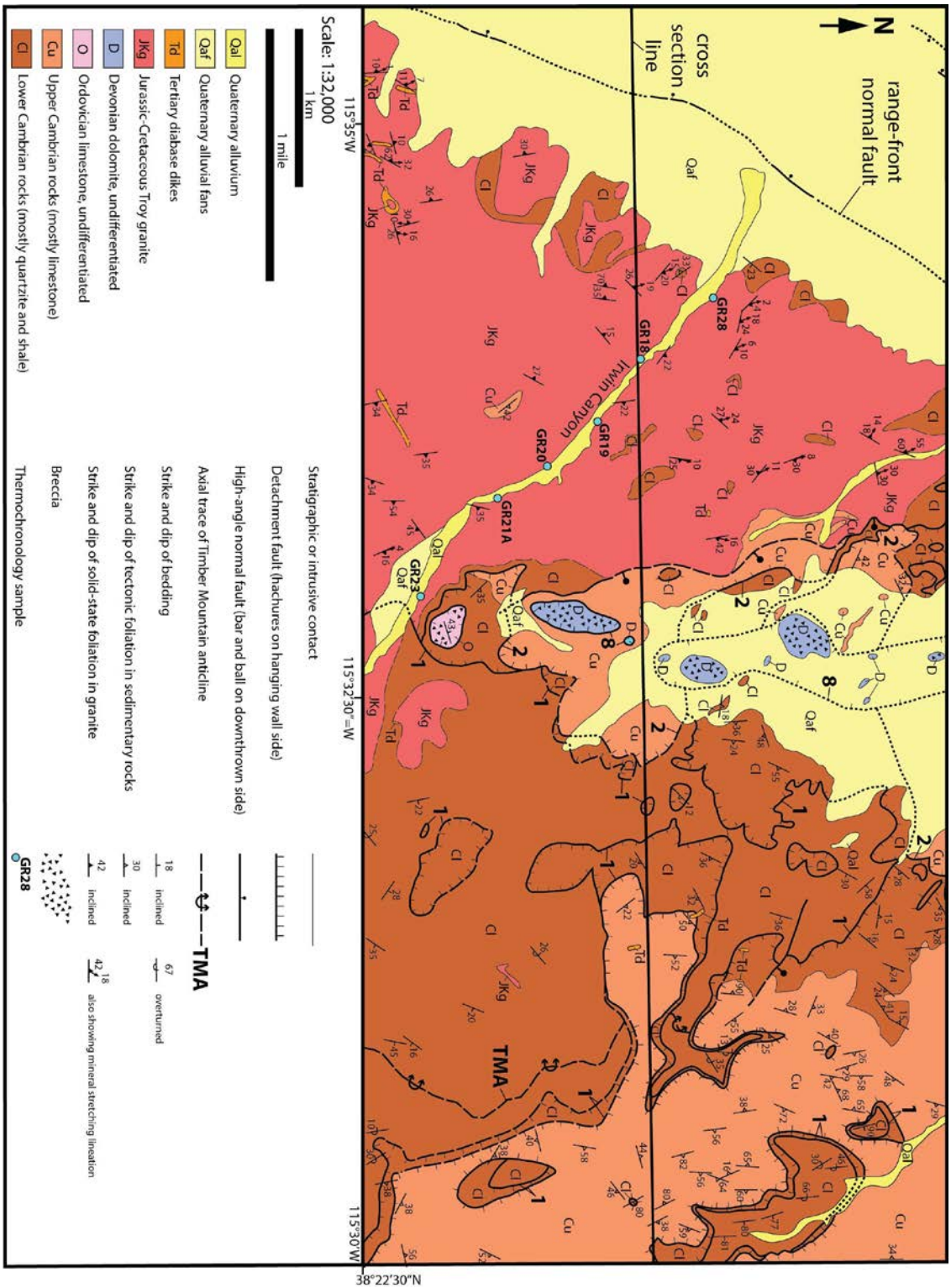

Text S3. Supporting data for oil wells in southern Railroad Valley.

Nine oil wells were projected onto cross section A-A′ (Fig. 3 in the text), and their locations are shown on Figure S2. Lithologic logs for these wells, which show intersection depths of the upper contacts of rock units (formation tops) as interpreted by the original well site geologists, are compiled in Hess et al. (2004), and individual lithologic and geophysical well logs are publicly available at the Great Basin Science Sample and Records library in Reno, NV. Formation top interpretations used in this study are summarized in Table S2. Logs of apparent dip magnitude were available at the Great Basin Science Sample and Records Library for two of these wells (RV10, QFC1).

Figure S2. Locations of the oil wells projected onto cross-section A-A′.

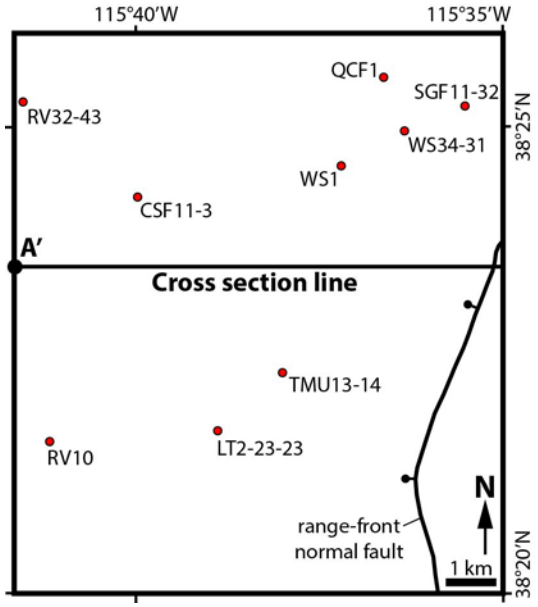

Table S2. Lithologic logs of wells in southern Railroad Valley.

Well abbreviation	Well name	Elevation	UTM N	UTM E	Interpreted formation tops (depths in feet)
SGF11-32	South Grant Federal No. 11-32	4730	4253200	623000	Neogene valley fill to 4490', Devonian to 4520', Jurassic-Cretaceous granite to total depth of 4681'
WS34-31	Willow Springs No. 34-31	4709	4252700	621800	Neogene valley fill to 5187', Devonian to 5464', Jurassic-Cretaceous granite to total depth of 5500'
QFC1	Quinn Canyon Federal No. 1	4708	4253750	621370	Neogene valley fill to 3995', Devonian to total depth of 4301'
WS1	Willow Spring No. 1	4704	4251981	620563	Neogene valley fill to 1454', Pliocene basalt to 1785', Neogene valley fill to 3814', Paleogene to 3959', Devonian to total depth of 4715'
TMU13-14	Timber Mountain Unit No. 13-14	4795	4247880	619400	Neogene valley fill to 2388', Paleogene to 3751', Devonian to total depth of 3943'
LT2-23-23	Lone Tree No. 2-23-23	4766	4246683	618142	Neogene valley fill to 2412', Paleogene to 3,365', Devonian to total depth of 4519'
CSF11-3	Christian Springs Federal No. 11-3	4707	4251300	616510	Neogene valley fill to 2006', Pliocene basalt to 2194', Neogene valley fill to 4678', Devonian to total depth of 5015'
RV10	Railroad Valley No. 10	4737	4246454	614826	Neogene valley fill to 4964', Paleogene to total depth of 5753'
RV32-43	Railroad Valley No. 32-43	4709	4253150	614230	Neogene valley fill to 2113', Pliocene basalt to 2195', Neogene valley fill to 4622', Paleogene to 5308', Devonian to total depth of 5988'

Text S4. Data supporting retro-deformation of tilting accommodated by set 2 normal faults.

The magnitude of tilting accommodated by motion on set 2 normal faults was estimated by summing their cumulative offset magnitude on cross section A-A′ (Table S3), after the methodology of Long and Walker (2015). Westward tilting accommodated by down-to-east faults was interpreted to have directly counteracted eastward tilting accommodated by down-to-west faults. Therefore, the total down-to-east offset magnitude was subtracted from the total down-to-west offset magnitude to generate a cumulative offset estimate. Across the full width of the cross section, the cumulative offset of set 2 faults is 2.23 km of down-to-west motion (Table S3). If the Grant Range and Railroad Valley are treated as a coherent block with a present-day width of 31.4 km, which pivoted from its western end, the magnitude of eastward tilting can be estimated either by solving trigonometrically, assuming an average fault orientation of 60˚W, or by solving for the geometry of a circle with a radius of 31.4 km and a radial rotation of 2.23 km (Fig. S3). Both techniques yielded similar results of ~4˚ of eastward rotation. This method assumes that tilt magnitude was homogeneous across the width of the cross section and that tilting accommodated by normal faults to the east and west of the cross section is negligible, and should therefore be considered approximate.

The 4˚ eastward rotation magnitude is corroborated by apparent dip data within Neogene valley fill sediment in two oil wells projected onto the cross section (Fig. 3 in the text). Well RV10 is characterized by gentle (typically <5°) eastward and westward apparent dip magnitudes between 0.5 and 1.25 km elevation. Well QFC1 is characterized by ~3-5˚ eastward apparent dip magnitudes between 0.5 and 1.2 km elevation. At lower elevations within these wells, as the contact with Paleozoic bedrock is approached, both wells exhibit progressively steeper eastward apparent dips, which is characteristic of syn-extensional deposition in half-grabens (e.g., Leeder and Gawthorpe, 1987). In addition, within the Neogene valley fill, a sub-horizontal basalt flow of likely Pliocene age (Johnson, 1993; Hulen et al., 1994) is intercepted at ~800-900 m elevation in three wells that span much of the width of the valley. The presence of a sub-horizontal basalt flow corroborates the shallow dips observed in the Neogene valley fill in wells RV10 and QFC1.

Table S3. Offset magnitudes of set 2 normal faults on cross section A-A′, from west to east.

Location	Fault offset (m)	Fault offset sense	Approximate dip angle
Railroad Valley	150	down-to-east	60˚ E
Railroad Valley	490	down-to-west	60˚ W
Railroad Valley	450	down-to-west	60˚ W
Railroad Valley	450	down-to-east	60˚ E
range-bounding fault	1585	down-to-west	70˚ W
Western Grant Range	885	down-to-east	60˚ E
Eastern Grant Range	275	down-to-west	59˚ W
Eastern Grant Range	245	down-to-west	60˚ W
Eastern Grant Range	670	down-to-west	59˚ W
cumulative:	**2230**	**down-to-west**	

Figure S3. Geometric models used to estimate tilt magnitude accommodated by set 2 normal faults on cross section A-A′. The top model shows rotation estimated by cumulative slip along a 60˚ west-dipping normal fault, and the bottom model shows rotation about a pivot located at the western end.

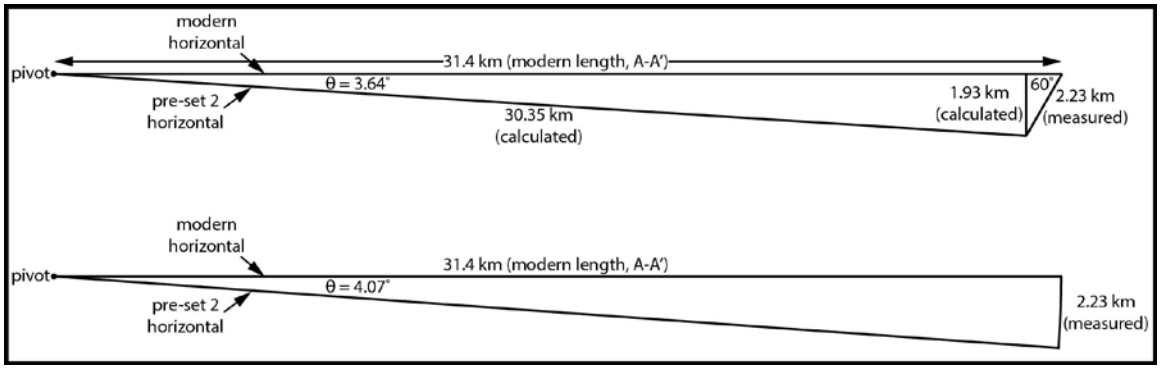

Text S5. Descriptions of geometric constraints, offset magnitudes, and field relationships of set 1 detachment faults.

Fault 1: Multiple traces of Fault 1 are exposed in the western third of the range, over an across-strike distance of 4 km (Fig. S1). In most exposures, Fault 1 consists of two subparallel faults that bound a ~20-30 m-thick sheet of lower Cambrian rocks; due to their close spacing, these two faults are simplified as one fault on cross section A-A′. Fault 1 places lower and upper Cambrian rocks over lower Cambrian rocks. Based on offset of the contact between lower and upper Cambrian rocks, Fault 1 has an estimated top-down-to-west offset magnitude of 11,000 feet (3,350 m). Fault 1 is cut in several places by Fault 2, at and south of the cross section line (Fig. S1). Four traces of Fault 1 intersect the cross section line (Fig. S1), and provide evidence for open, anticlinal folding

of the fault surface (Fig. 3 in the text). Between the easternmost two traces, a dip of 5°E is defined. Between the two middle traces, a dip of 10°W is defined. Between the westernmost two traces, a dip of 12°W is defined. Below the modern erosion surface to the east of its easternmost trace, the dip angle of Fault 1 is unconstrained. After observations of 4-5° cutoff angles with stratigraphy documented on several set 1 faults in the eastern half of the range (see descriptions of Faults 4-7 below), a cutoff angle of 5° was assumed in the subsurface for Fault 1, which corresponds to subsurface dip magnitudes ranging between 0-25°E. Cutoff angles observed for portions of Fault 1 that deform the Timber Mountain anticline are high. Footwall cutoff angles vary between 100-118° above the overturned limb of the anticline, and are between 42-80° in the subsurface to the east, above the eastern flank of the anticline. Footwall cutoff angles are between 29-46° above the upright limb of the anticline, and hanging wall cutoff angles are between 42-57°.

Fault 2: On cross section A-A′ (Fig. 3 in the text), separate western and eastern exposures of Fault 2 are interpreted to connect above the modern erosion surface. The western exposure dips to the west and places upper Cambrian rocks over lower Cambrian rocks (Fig. S1). The eastern exposure, which was mapped by Hyde and Huttrer (1970) and Lund et al. (1988), dips to the east and places Ordovician rocks over upper Cambrian rocks. Evidence supporting correlation of these two fault exposures includes: 1) these two faults define the structurally next-highest faults above Fault 1 on the east and west, and a continuous exposure of upper Cambrian rocks in the hanging wall of Fault 1 that is undisturbed by faulting lies between them; 2) the map units juxtaposed on either side of both fault exposures define a similar top-to-west offset magnitude, and therefore correlation of these two faults is kinematically compatible; and 3) the folding observed on Fault 1 implies that the overlying Fault 2 is also folded, after field relations described ~6 km to the north in Long and Walker (2015). Therefore, the simplest kinematic interpretation is that these two fault exposures connect above the erosion surface as one fault. Based on offset of the contact between lower and upper Cambrian rocks, Fault 2 has an estimated top-to-west offset magnitude of 12,200 feet (3,720 m). At its western exposure, Fault 2 cuts Fault 1 at and south of the cross section line (Fig. S1). In addition, field relationships imply that Fault 2 is cut by Fault 8 (Fig. S1). Two hundred meters north of the cross section line, lower Cambrian rocks in the footwall of Fault 2 are overlain by Devonian rocks in the hanging wall of Fault 8. However, ~100 m south of the cross section line, upper Cambrian rocks in the hanging wall of Fault 2 are overlain by Devonian rocks in the hanging wall of Fault 8. These relationships imply that Fault 2 is cut by Fault 8 within the intervening region of Quaternary sediments (Fig. S1). At its eastern exposure, Lund et al. (1988) showed that Fault 2 is cut by Fault 3 approximately 4.5 km north of the cross section line. At its western exposure, Fault 2 has to dip 11-13 °W (or steeper) in order to not intersect the modern erosion surface to the east and west of its trace. A three-point problem calculated on its trace along the cross section line defines a strike of 015°, and an elevation drop of 100 feet over a lateral distance of 325 feet, corresponding to a 17° westward dip. At its eastern exposure, Fault 2 has to dip at least 10°E in order to not intersect the modern erosion surface to the west of its trace. In

the subsurface to the east of its eastern trace, the dip of Fault 2 is unconstrained; however assuming a cutoff angle of 5° (see discussion above for Fault 1, and see descriptions below for Faults 3-7), dips between 0-25°E are estimated in the subsurface. Cutoff angles observed for the western exposure of Fault 2, which deforms the eastern flank of the Timber Mountain anticline, vary between 20-64°.

Fault 3: Fault 3 was mapped by Hyde and Huttrer (1970) and Lund et al. (1988), and places the upper part of the Ordovician section over the lower part of the Ordovician section. Based on westward offset of the upper and lower contacts of the Ordovician Eureka quartzite, Fault 3 has an estimated top-to-west offset magnitude of 10,000 feet (3,050 m). Approximately 4.5 km north of the cross section line, Fault 3 cuts Faults 2 (Lund et al., 1988). To the north, Hyde and Huttrer (1970) map Fault 3 as far north as Heath Canyon, where it correlates with Fault 5 of Long and Walker (2015). Fault 3 must dip at least 5°E in order to not intersect the modern erosion surface to the west of its trace. Fault 3 is shown at a dip of 25°E, which is based on assumption of a 5° cutoff angle with stratigraphy (see discussion for Faults 3-7 below). Its geometry above the erosion surface to the west of its trace is unconstrained.

Fault 4: Fault 4 was mapped by Lund et al. (1988), and places the base of the Devonian section over the Silurian section. Measurement of the offset of the contact between Devonian and Silurian rocks yields a top-to-west offset estimate of 9,800 feet (2,990 m). Lund et al. (1988) mapped Faults 3 and 4 merging ~2 km north of the cross section line. Fault 4 must dip at least 10°E to not intersect the modern erosion surface to the west of its trace. However, assuming that its cutoff angle with stratigraphy remains constant across-strike, Fault 4 cannot have a cutoff angle higher than 5° without intersecting the modern erosion surface in the westernmost flank in the range. Therefore, Fault 4 is drawn with a 5° cutoff angle, which corresponds to a 25°E dip at the modern erosion surface. The geometry of Fault 4 above the erosion surface to the west of its trace is unconstrained; however field relationships indicate that it merges with Fault 3 (Lund et al., 1988).

Fault 5: Fault 5 was mapped by Lund et al. (1988), and places upper Devonian rocks over lower Devonian rocks. Fault 5 is not exposed on the cross section line, and is shown in the subsurface only; its position on the cross section was projected southward from its trace mapped ~2.0 km to the north of the cross section line by Lund et al. (1988), where it is cut by Fault 7. The existence of Fault 5 in the subsurface is required by the map units exposed in the footwall of the two traces of Fault 7. The western trace of Fault 7 places Paleogene rocks over Devonian rocks, and the eastern trace places Paleogene rocks over Mississippian rocks. To accomplish this stratigraphic omission in the footwall of Fault 7, Faults 5 and 6 are shown merging upward with Fault 7 between its two traces. This facilitates omission of much of the Mississippian section and the upper part of the Devonian section, and is kinematically compatible with the geometries and relative unit juxtapositions of Faults 5 and 6. Based on the westward offset of the contact between Devonian and Mississippian rocks, top-to-west offset on Fault 5 is estimated at 11,500

feet (3,510 m). The location of its intersection with Fault 6 is estimated from southward projection of its trace ~2 km to the north of the cross section line on Lund et al. (1988). East of this intersection, the cutoff angle with stratigraphy of Fault 5 cannot exceed 4° without intersecting the modern erosion surface in the footwall of the easternmost set 2 normal fault. This corresponds to dips between 10-15°E near the modern erosion surface.

Fault 6: Fault 6 was mapped by Kleinhampl and Ziony (1985), and places Pennsylvanian rocks over Mississippian rocks. This fault likely correlates with Fault 8 of Long and Walker (2015), which is mapped ~6 km to the north. This contact was mapped as depositional by Lund et al. (1988), Hyde and Hutter (1970), and Scott (1965). However, we argue that the existence of this fault is supported by the 550' thick section of Mississippian Chainman shale exposed in its footwall, which we interpret as tectonically-thinned, as this unit is as thick as 1250-1400' in nearby areas of the Grant Range (Hyde and Huttrer, 1970; Long and Walker, 2015). Offset on Fault 6, as estimated from top-to-west offset of the contact between Mississippian and Pennsylvanian rocks, is 5,700 feet (1,740 m). Fault 6 must dip at least 12°E to not intersect the modern erosion surface to the east of its trace, corresponding to a maximum permissible cutoff angle with stratigraphy of 13°. However, in order to intersect the structurally-higher Fault 7 east of its western trace (which is required by field relations, as a structure that can be correlated with Fault 6 is not observed in the footwall of Fault 7), the cutoff angle on Fault 6 is limited to a maximum of 5° (assuming that cutoff angles remain constant across strike). Therefore, Fault 6 is shown with a cutoff angle of 5°, corresponding to a dip of 20°E at its trace. In the hanging wall of Fault 6, a ~150 foot-thick section of the Pennsylvanian Ely limestone is unconformably overlain by a ~4000 foot-thick section of Paleogene volcanic and sedimentary rocks. With the geometry shown, Fault 6 cuts Paleogene units as young as the ~31.2 Ma Windous Butte Formation on the area of the cross section.

Fault 7: Fault 7 was mapped by Lund et al. (1988), and places Paleogene rocks over Devonian rocks. Based on the westward offset of the contact between Mississippian and Paleogene rocks, a top-to-west offset magnitude of 3,000 feet (910 m) is estimated for Fault 7. As a result of set 2 normal faulting, two traces of Fault 7 intersect the modern erosion surface on the cross section. Connecting its two traces yields a cutoff angle with stratigraphy of 4° and a dip angle of 16°E. To the west of its western trace, Fault 7 has to dip at least 12°E in order to not intersect the modern erosion surface. To the west of its western trace, cutoff angles on Fault 7 cannot be greater than 4° without intersecting the modern erosion surface (assuming constant cutoff angles across strike). Therefore, this limits the dip angle west of its western trace to a minimum of 16°E. To the east of its eastern trace, the cutoff angle on Fault 7 is increased to 12°, in order to not intersect the modern erosion surface on the area of the cross section (Fig. 3 in the text). Along its eastern trace, Fault 7 cuts Paleogene volcanic units as young as the ~27.2-29.7 Ma Needles Range Formation.

Fault 8: In the western Grant Range, Fault 8 places brecciated Devonian limestone over upper Cambrian rocks in the hanging wall of Fault 2, and over lower Cambrian rocks in

the hanging wall of Fault 1 (Fig. S1). Though the contact is concealed under Quaternary sediment, these field relationships require that Fault 8 cuts Fault 2. Fault 8 is correlated with an additional fault intercepted in the two easternmost drill holes in Railroad Valley (SGF11-32, WS34-31), which places Devonian rocks over Jurassic-Cretaceous granite. This fault is correlated with the exposure of Fault 8 in the western Grant Range because they both carry Devonian rocks in their hanging wall. On the cross section, Fault 8 is shown cutting structurally-downward toward the west, and cutting Fault 2 just to the east of the range front normal fault. This relationship allowed for Jurassic-Cretaceous granite to lie in the footwall of Fault 8, which is observed in the drill holes. In the western Grant Range, Fault 8 is exposed ~100 m south of the cross section line, which implies that it is just above the modern erosion surface. To the east of its trace, Fault 8 cannot dip any shallower than 9°W without intersecting the modern erosion surface. Between its trace and the interception of Fault 8 in well SGF11-32, a dip of 22°W is defined, which corresponds to a 3° hanging wall cutoff angle. The footwall cutoff angles here are high (48-69°), as these rocks restore to the eastern flank of the Timber Mountain anticline. Between its intersections in wells SGF11-32 and WS34-31, a dip of 14°W is defined. Dip data are not available for either of these wells, and therefore cutoff angles cannot be accurately estimated here. However, a hanging wall cutoff angle of 3° is shown between these two wells, to match the cutoff angle observed in the western Grant Range. West of its intersection with well WS34-31, the subsurface geometry of Fault 8 is unconstrained; it is shown shallowing in dip, and staying just below the total depth of the wells. Rocks that can be matched up between the footwall and hanging wall of Fault 8 are not present on the area of the cross section. Between well WS34-31 and the easternmost trace of Fault 8 in the Grant Range, 15,900 feet (4,850 m) of minimum structural overlap is estimated. As the geometry of Fault 8 is not constrained west of well WS34-31, structural overlap from here to point A'' at the western edge of the cross section, which is 22,500 feet (6,860 m), should be considered approximate. Cross cutting relationships between Fault 8 and Faults 3-7 in the eastern part of the range are not exposed. Fault 8 carries rocks that are stratigraphically-higher than Faults 3 and 4, so it is likely that they do not correlate. Fault 8 carries rocks that are at similar stratigraphic levels to those carried by Fault 7; however, the east-west extent of Devonian rocks preserved in the hanging wall of Fault 8, combined with the Devonian position of the Paleogene unconformity in Railroad Valley, indicate that rocks in the hanging wall of Fault 8 restore stratigraphically higher than Fault 7 (Fig. 3C in the text), and therefore Fault 8 represents a separate and structurally-higher fault.

Stratigraphic omission across Fault 8 at wells SGF11-32 and WS34-31 is at least 8,600-9,200 m, which is the largest omission in the study area. Therefore, we interpret that Fault 8 represents a 'master' detachment level, into which the cumulative offset from all of the older, structurally-lower faults to the east was fed (e.g., Long and Walker, 2015). Thus, as faults are successively crossed from east to west, cumulative offset on Fault 8 increases, as well as stratigraphic omission. The cumulative offset magnitude of Faults 1-7 is 19,270 m, which is sufficient to account for the 11,710 m of minimum structural overlap observed across Fault 8. The restored position of the rocks in the hanging wall of

Fault 8 require an additional 4,300 m of offset on this fault, in order to place point A′ over A′′.

Text S6. Mineral separation methods

Standard mineral separation procedures were used to obtain zircon, apatite, and muscovite fractions from the eight Irwin Canyon granite samples. These included crushing and pulverizing whole rock samples to sand-size grains, density separation on a Wilfley table, separation into dense and light fractions by heavy liquid separation, and passing the dense fraction through a Frantz magnetic separator.

Text S7. Supporting data for muscovite $^{40}Ar/^{39}Ar$ ages and multi-diffusion domain modeling

$^{40}Ar/^{39}Ar$ analyses of the eight Irwin Canyon granite samples were performed at the New Mexico Geochronology Research Laboratory. Approximately 3 mg of each sample were wrapped in copper foil and placed in a 24-hole, 2.54 cm diameter aluminum disk along with neutron flux monitor FC-2 sanidine (28.201 Ma; Kuiper et al., 2008) placed in every third hole around the disk. The package was irradiated in the central thimble at the United States Geological Survey TRIGA reactor located in Denver, CO. The muscovite samples were step-heated in the double-vacuum Nb resistance furnace with a heating time of 18 minutes for each increment. The evolved gases were exposed to a SAES GP-50 getter (operated at 450°C) during heating. Following heating, gas was expanded into a second stage and reacted for 1.5 minutes with two SAES GP-50 getters, one heated to 450 °C and the other at room temperature. Gas was also exposed to a W filament operated at 2000 °C while in the second stage. Argon isotopes were analyzed with a MAP 215 50 mass spectrometer fitted with a Balzers 217 multiplier operated in analogue mode. Blanks were run at room temperature and are generally not temperature-dependent below about 1150 °C and averaged 85±35%, 1.0±2.5%, 0.2±8%, 0.08±3%, and 0.06±15% moles $x10^{-17}$ for masses 40, 39, 38, 37, and 36, respectively. All samples were heated to 1620 °C, but in many instances the samples were fully degassed by about 1100 °C and the higher temperature steps are not reported. J-factors were determined to a precision of ~0.1% by single crystal fusion of 6 grains in each of 8 irradiation locations. Analytical data are provided in Table S4.

Table S4 (following 6 pages). $^{40}Ar/^{39}Ar$ analytical data for the Irwin Canyon granite samples.

ID	Temp (°C)	$^{40}Ar/^{39}Ar$	$^{37}Ar/^{39}Ar$	$^{36}Ar/^{39}Ar$ (x 10^{-3})	$^{39}Ar_K$ (x 10^{-15} mol)	K/Ca	$^{40}Ar^*$ (%)	^{39}Ar (%)	Age (Ma)	±1σ (Ma)	Time (min)
GR 18, Muscovite, 3.74 mg, J=0.0018251±0.08%, D=1.005±0.001, NM-268L, Lab#=63065-01											
A	550	89.51	0.01	277.3	1.23	51.1	8.5	0.7	25.1	2	18
B	600	25.58	-0.0019	59.76	1.133	-	30.9	1.3	26.2	1.5	18
C	650	24.49	0.0012	55.88	2.045	412.8	32.6	2.5	26.45	0.86	18
D	685	20.83	0.0002	44.71	2.436	2727	36.5	3.9	25.25	0.74	18
E	720	23.56	-0.0008	54.35	3.692	-	31.8	6	24.87	0.58	18
F	740	23.4	-0.0017	52.77	5.001	-	33.3	8.8	25.88	0.45	18
G	750	17.63	-0.0015	32.66	5.308	-	45.2	11.8	26.45	0.38	18
H	760	16.28	-0.001	27.19	6.287	-	50.6	15.3	27.33	0.32	18
I	770	14.44	0	21.54	7.199	13462	55.9	19.4	26.75	0.28	18
J	775	12.96	0	16.66	6.924	17413	62	23.3	26.62	0.27	18
K	780	12.26	0.0001	14.68	6.637	4196	64.6	27.1	26.25	0.27	18
L	790	12	-0.0006	13.28	7.444	-	67.3	31.3	26.77	0.25	18
M	795	11.32	-0.0016	10.73	6.558	-	72	35	27.01	0.26	18
N	800	11.01	-0.001	10.12	5.751	-	72.8	38.2	26.56	0.3	18
O	810	11.03	-0.0005	10	5.8	-	73.2	41.5	26.75	0.29	18
P	820	11.28	0	10.58	5.317	32916	72.3	44.5	27.02	0.32	18
Q	830	11.5	-0.0016	11.72	4.95	-	69.9	47.3	26.65	0.34	18
R	840	11.97	0.0001	13.09	4.405	4555	67.7	49.8	26.85	0.39	18
S	850	12.76	-0.0021	15.32	3.926	-	64.5	52	27.27	0.43	18
T	860	13.55	-0.0016	17.94	3.52	-	60.8	54	27.32	0.48	18
U	870	14.53	-0.0025	20.71	3.136	-	57.9	55.8	27.85	0.54	18
V	890	15.43	-0.0017	23.21	3.566	-	55.5	57.8	28.38	0.5	18
W	915	15.94	0.0012	24.12	4.874	438.8	55.3	60.5	29.19	0.39	18
X	930	16.31	-0.0012	24.51	5.065	-	55.6	63.4	30.02	0.37	18
Y	945	16.36	0.0003	24.69	5.313	1786.4	55.4	66.4	30	0.36	18
Z	960	16.53	-0.0018	25.23	5.828	-	54.9	69.7	30.05	0.32	18
AA	975	16.23	-0.0008	23.34	6.821	-	57.5	73.5	30.9	0.3	18
AB	990	14.45	0.0011	17.27	10.052	457	64.7	79.2	30.95	0.21	18
AC	1035	11.12	0	6.341	22.91	16673	83.1	92.2	30.598	0.1	18
AD	1050	10.05	0.0007	2.872	11.156	728.2	91.6	98.5	30.47	0.16	18
AE	1090	11.37	-0.0039	8.579	2.709	-	77.7	100	29.25	0.6	18
Integrated age ± 1σ			n=31		177			K2O=9.96%	28.26	0.12	
Plateau ± 1	steps AA-AE		n=5	MSWD=2.38	53.64			30.3	30.61	0.118	
GR 19, Muscovite, 2.43 mg, J=0.0018227±0.08%, D=1.005±0.001, NM-268L, Lab#=63066-01											
A	550	49.14	0.1634	135.7	1.162	3.1	18.4	1.1	29.9	1.6	18
B	600	21.51	0.084	46.28	1.284	6.1	36.4	2.4	25.9	1.3	18
C	650	16.37	0.0251	28.74	2.06	20.3	48.1	4.4	26.09	0.81	18
D	685	14.87	0.0199	23.97	2.549	25.6	52.4	6.9	25.79	0.67	18
E	720	14.84	0.0082	23.1	3.562	62.3	54	10.4	26.53	0.51	18
F	740	14.21	0.0086	20.32	3.755	59.3	57.7	14.1	27.17	0.46	18

G	750	13.81	0.0034	18.8	3.62	152.1	59.8	17.7	27.32	0.48	18
H	760	13.08	0.0046	15.69	3.906	111.6	64.5	21.5	27.93	0.45	18
I	770	12.59	0.001	14.21	4.198	496	66.6	25.6	27.76	0.4	18
J	775	11.99	-0.0002	12.38	3.761	-	69.5	29.3	27.56	0.45	18
K	780	11.68	0.0033	11.7	3.477	152.6	70.4	32.7	27.21	0.48	18
L	790	11.42	0.0004	10.83	3.808	1169	72	36.5	27.21	0.44	18
M	795	11.34	-0.002	10.82	3.349	-	71.8	39.8	26.94	0.49	18
N	800	11.18	-0.0007	10.29	3.003	-	72.8	42.7	26.94	0.55	18
O	810	11.15	0.0001	10.06	3.108	7719	73.3	45.8	27.05	0.53	18
P	820	11.27	0.0004	11.34	3.069	1189	70.2	48.8	26.21	0.54	18
Q	830	11.3	0.0004	10.72	2.98	1336	71.9	51.7	26.91	0.55	18
R	840	11.59	0.0009	11.59	2.837	583.5	70.4	54.5	27.03	0.58	18
S	850	11.89	-0.0002	11.94	2.663	-	70.3	57.1	27.65	0.63	18
T	860	12.21	-0.0008	13.05	2.514	-	68.4	59.6	27.65	0.66	18
U	870	12.64	0.0006	14.34	2.355	821.3	66.5	61.9	27.81	0.7	18
V	890	12.8	0.0023	14.9	2.775	219.3	65.6	64.6	27.8	0.62	18
W	915	12.64	0.0031	14.07	3.826	165.7	67.1	68.4	28.08	0.45	18
X	930	13.04	0.0014	14.45	3.667	367.2	67.2	72	29	0.47	18
Y	945	13.88	0.0017	17.06	3.247	297.7	63.7	75.1	29.24	0.54	18
Z	960	14.62	0.0032	18.55	3.173	160.3	62.5	78.3	30.22	0.53	18
AA	975	14.86	0.0012	18.59	3.367	423.4	63	81.6	30.95	0.51	18
AB	990	14.89	0.0029	18.68	3.932	174.9	62.9	85.4	30.99	0.46	18
AC	1035	12.88	0.0032	9.724	9.994	160.6	77.7	95.2	33.05	0.19	18
AD	1050	11.88	0.0087	6.967	3.267	58.4	82.7	98.4	32.45	0.5	18
AE	1090	19.5	0.0406	28	0.731	12.6	57.6	99.2	37.1	2.2	18
AG	1620	47.36	0.0738	114	0.858	6.9	28.9	100	45	2.1	18
Integrated age ± 1σ			n=32		101.86			K2O=8.83%	28.68	0.13	
Plateau ± 1	steps AC-AE		n=3	MSWD=2.30	13.99			13.7	33	0.28	

GR20, Muscovite, 3.65 mg, J=0.0018297±0.07%, D=1.005±0.001, NM-268L, Lab#=63064-01

A	550	48.89	0.0151	140.5	1.082	33.8	15.1	0.7	24.6	1.6	18
B	600	20.68	0.0147	45.5	1.027	34.6	35	1.3	24.1	1.4	18
C	650	15.7	0.0002	29.49	1.992	2520	44.5	2.5	23.22	0.69	18
D	700	14.84	0.0013	26.54	3.504	388	47.1	4.7	23.27	0.44	18
E	720	14.54	0.0034	24.8	3.088	150.6	49.6	6.6	23.97	0.45	18
F	750	15.51	0.003	26.46	4.563	172.3	49.6	9.4	25.56	0.35	18
G	760	14.1	0.0014	21	4.4	353.8	56	12.1	26.22	0.35	18
H	770	13.25	0.0003	17.67	4.79	1740	60.6	15	26.69	0.31	18
I	775	12.5	0.0013	15.9	4.296	386.5	62.4	17.7	25.94	0.33	18
J	785	12.17	-0.0008	14.28	4.599	-	65.3	20.5	26.41	0.31	18
K	790	11.29	0	12.06	4.221	12755	68.4	23.1	25.66	0.34	18
L	800	11.52	-0.0009	12.51	4.518	-	67.9	25.8	25.99	0.31	18
M	820	11.13	0.0007	10.47	6.332	768	72.2	29.7	26.69	0.23	18
N	850	10.7	0.0008	8.704	10.465	645.2	75.9	36.2	27	0.17	18
O	870	10.79	0.0022	9.209	8.935	231.2	74.8	41.7	26.82	0.17	18
P	890	11.75	0.0007	11.58	7.614	701.5	70.9	46.3	27.67	0.2	18
Q	910	12.62	0.0007	13.52	6.997	725.5	68.3	50.6	28.62	0.23	18

R	930	12.89	0.0007	14.24	7.196	773.9	67.4	55	28.84	0.23	18
S	950	12.58	-0.0005	12.66	7.554	-	70.2	59.7	29.34	0.2	18
T	980	12.4	0.0005	12.18	9.345	1037	71	65.4	29.23	0.18	18
U	1010	12.49	0.0013	12.02	10.681	381.3	71.5	72	29.67	0.17	18
V	1040	12.69	0.0004	12.4	15.03	1420	71.1	81.2	29.96	0.14	18
W	1070	11.18	0.0004	6.986	18.75	1367	81.5	92.7	30.26	0.1	18
X	1110	9.631	0.0002	3.038	6.789	2767	90.7	96.9	29	0.2	18
Y	1620	13.04	0.0271	13.61	5.053	18.8	69.2	100	29.96	0.29	18
Integrated age ± 1σ			n=25		262.8			K2O=9.36%	27.999	0.095	
Plateau ± 1	steps V-Y		n=4	MSWD=10.28	45.62			28	29.99	0.239	

GR 21A, Muscovite, 3.42 mg, J=0.0018405±0.08%, D=1.005±0.001, NM-268L, Lab#=63060-01

A	550	100.9	0.0444	306.8	1.212	11.5	10.2	0.8	34.2	2.1	18
B	600	26.14	0.0312	58.12	1.045	16.4	34.3	1.5	29.9	1.4	18
C	650	20.36	0.0257	40.27	1.885	19.9	41.5	2.8	28.26	0.81	18
D	700	17.8	0.0152	31.63	3.288	33.5	47.5	5	28.25	0.49	18
E	720	15.41	0.0108	22.38	2.955	47.4	57.1	7.1	29.37	0.52	18
F	750	17.34	0.0074	27.15	4.942	69.4	53.7	10.4	31.09	0.8	18
G	770	18.12	0.0018	24.52	5.941	290.7	60	14.4	36.26	0.3	18
H	775	15.44	0.0032	16.41	5.254	161.3	68.6	18	35.32	0.3	18
I	785	15.58	0.0037	15.69	6.026	136.1	70.2	22.1	36.48	0.27	18
J	790	14.2	0.003	12.02	5.403	171.8	75	25.8	35.51	0.28	18
K	800	14.33	0.0011	11.21	5.902	453	76.9	29.8	36.72	0.28	18
L	820	13.97	0.0018	9.365	8.824	285.6	80.2	35.8	37.33	0.18	18
M	850	12.9	0.0021	8.049	10.993	244.3	81.6	43.3	35.1	0.16	18
N	870	13	0.0027	9.164	7.432	190.4	79.2	48.3	34.32	0.21	18
O	890	15.07	0.0028	12.33	5.618	179.8	75.8	52.1	38.08	0.28	18
P	910	17.78	0.0032	15.65	4.511	159	74	55.2	43.78	0.34	18
Q	920	19.8	0.0047	17.39	3.391	108.7	74	57.5	48.71	0.44	18
R	930	20.45	0.0048	16.92	3	106.9	75.5	59.5	51.29	0.49	18
S	950	20.68	0.0024	16.54	3.558	214.4	76.4	61.9	52.44	0.42	18
T	980	20.47	0.0028	15	5.091	180.6	78.3	65.4	53.22	0.32	18
U	1010	21.38	0.0042	17.32	7.161	120.3	76.1	70.3	53.97	0.25	18
V	1040	19.7	0.0017	12.72	19.22	307.6	80.9	83.3	52.9	0.14	18
W	1070	17.57	0.0038	6.116	17.08	133.5	89.7	94.9	52.34	0.13	18
X	1110	17.04	0.0129	7.987	5.842	39.5	86.2	98.9	48.79	0.26	18
Y	1620	42.42	0.2903	109.6	1.657	1.8	23.7	100	33.6	1.1	18
Integrated age ± 1σ			n=25		147.2			K2O=8.98%	42.71	0.13	
Plateau ± 1	steps U-X		n=4	MSWD=82.2	49.31			33.5	52.35	0.766	

GR 23, Muscovite, 3.26 mg, J=0.001837±0.07%, D=1.005±0.001, NM-268L, Lab#=63062-01

A	550	76.21	0.0159	221.1	0.72	32.1	14.3	0.5	36.2	2.3	18
B	600	29.41	0.014	63.22	0.728	36.5	36.5	0.9	35.7	1.9	18
C	650	22.43	0.001	40.11	1.4	532.4	47.2	1.9	35.2	1	18
D	700	20.57	0.0048	33.02	2.605	106.9	52.6	3.6	35.99	0.59	18
E	720	21.8	0.0007	36.52	2.374	747.4	50.5	5.1	36.62	0.63	18
F	750	24.66	0.0021	40.24	4.09	246.1	51.8	7.8	42.41	0.44	18

G	770	23.38	0.0006	29.32	7.166	916.5	62.9	12.4	48.82	0.28	18
H	775	18.17	0.0002	17.76	5.787	2341	71.1	16.2	42.94	0.29	18
I	785	18.18	-0.0002	17.59	5.897	-	71.4	20.1	43.14	0.28	18
J	790	16.38	0.0002	11.72	4.929	2946	78.9	23.3	42.9	0.31	18
K	800	16.78	-0.0001	11.68	5.146	-	79.4	26.6	44.26	0.29	18
L	820	17.18	0.0008	10.06	7.324	651.3	82.7	31.4	47.15	0.22	18
M	850	17.48	-0.0003	9.012	10.479	-	84.8	38.3	49.13	0.17	18
N	870	19.37	0.0013	11.21	7.143	383.1	82.9	42.9	53.18	0.22	18
O	890	23.52	0.0021	14.7	5.671	248.3	81.5	46.6	63.34	0.28	18
P	910	27.14	0.0008	17.08	5.229	600.5	81.4	50	72.8	0.32	18
Q	930	28.05	0.0026	17.26	5.516	198.9	81.8	53.6	75.56	0.31	18
R	950	27.33	-0.0004	15.62	6.112	-	83.1	57.6	74.82	0.28	18
S	980	26.81	0.0012	14.99	8.197	416.7	83.5	63	73.75	0.24	18
T	1010	26.52	0.0015	15.86	13.02	330.1	82.3	71.5	71.98	0.2	18
U	1040	23.7	0.0002	8.221	23.97	3379	89.7	87.1	70.15	0.14	18
V	1070	21.4	0.0006	2.132	12.58	837.4	97.1	95.3	68.51	0.16	18
W	1110	21.16	0.0013	2.088	4.837	380.7	97.1	98.5	67.79	0.29	18
X	1620	27.36	0.0252	23.6	2.359	20.3	74.5	100	67.3	0.61	18
Integrated age ± 1σ			n=24		153.3			K2O=9.83%	59.89	0.13	
Plateau ± 1	steps T-X		n=5	MSWD=64.69	56.76			37	69.73	0.692	

GR25, Muscovite, 5.1 mg, J=0.0018327±0.07%, D=1.005±0.001, NM-268L, Lab#=63063-01

A	550	34.55	0.0861	91.92	1.842	5.9	21.4	0.8	24.62	1	18
B	600	18.56	0.0734	28.24	1.453	6.9	55	1.5	33.95	0.94	18
C	650	15.89	0.0119	17.65	2.453	42.9	67.2	2.6	35.46	0.57	18
D	700	14.7	0.0094	12.19	4.047	54.2	75.5	4.4	36.83	0.35	18
E	720	14.73	0.0082	9.728	3.605	61.9	80.5	6	39.34	0.41	18
F	750	16.84	0.0042	10.68	6.079	120.7	81.2	8.7	45.32	0.24	18
G	760	16.27	0.0033	7.911	5.811	156.3	85.6	11.4	46.15	0.25	18
H	770	16.22	0.0023	7.543	5.836	225.3	86.3	14	46.31	0.25	18
I	775	15.65	0.0013	6.446	5.086	391	87.8	16.3	45.51	0.28	18
J	785	16.17	0.0021	6.156	5.568	238.1	88.7	18.8	47.5	0.25	18
K	790	15.81	0.0011	5.762	4.841	469.6	89.2	20.9	46.71	0.29	18
L	800	16.24	0.0028	5.484	5.358	184.2	90	23.3	48.38	0.27	18
M	820	16.89	0.0009	5.377	8.314	591.5	90.6	27.1	50.62	0.19	18
N	850	17.12	0.0022	4.759	13.67	232.9	91.8	33.2	51.96	0.14	18
O	870	17.26	0.002	5.26	11.656	256	91	38.4	51.91	0.15	18
P	890	17.96	0.002	5.416	11.526	257.1	91.1	43.6	54.07	0.15	18
Q	890	18.58	0.0016	5.569	7.675	326.1	91.1	47.1	55.91	0.21	18
R	905	18.87	0.0023	5.205	8.825	222.2	91.8	51	57.21	0.18	18
S	930	19.17	0.002	4.485	13.52	254	93.1	57.1	58.88	0.15	18
T	950	19.76	0.0022	4.485	13.95	233.6	93.3	63.4	60.82	0.14	18
U	980	20.72	0.002	4.793	18.27	250.2	93.2	71.6	63.63	0.12	18
V	1010	21.49	0.0019	4.113	22.79	267.3	94.3	81.8	66.77	0.12	18
W	1040	20.97	0.0017	1.542	25.12	304.5	97.8	93.1	67.53	0.11	18
X	1070	20.66	0.0041	0.9559	12.56	124.5	98.6	98.7	67.11	0.15	18
Y	1110	21.11	0.0194	3.873	2.877	26.3	94.6	100	65.75	0.47	18

Integrated age ± 1σ			n=25		222.7			K2O=9.15%	56.676	0.094	
Plateau ± 1	steps W-Y		n=3	MSWD=8.42	40.567			18.2	67.32	0.254	
GR 27A, Muscovite, 2.98 mg, J=0.0018403±0.08%, D=1.005±0.001, NM-268L, Lab#=63059-01											
A	550	54.42	0.0257	140	1.183	19.8	24	0.8	43.5	1.6	18
B	600	29.06	0.0246	48.71	1.293	20.8	50.5	1.8	48.7	1.2	18
C	650	24.54	0.0145	31	2.262	35.3	62.7	3.4	51.08	0.7	18
D	700	25.66	0.0105	32.24	3.965	48.5	62.9	6.2	53.54	0.45	18
E	720	24.69	0.0075	26.42	3.646	67.8	68.4	8.8	55.99	0.47	18
F	750	25.94	0.0057	26.9	5.666	90.1	69.4	12.8	59.62	0.35	18
G	770	24.63	0.0052	19.72	7.204	97.8	76.3	18	62.24	0.28	18
H	775	23.51	0.0054	15.78	5.696	94.4	80.2	22	62.41	0.31	18
I	785	23.3	0.0039	13.95	5.457	129.3	82.3	25.9	63.47	0.31	18
J	790	23.37	0.0054	14.12	4.563	94.4	82.1	29.2	63.53	0.37	18
K	800	23.41	0.003	13.4	4.512	167.6	83.1	32.4	64.37	0.35	18
L	810	23.62	0.0049	13.24	4.363	105	83.4	35.5	65.19	0.37	18
M	820	23.78	0.0064	13.73	4.096	80.3	82.9	38.4	65.25	0.39	18
N	835	23.73	0.0048	13.27	4.506	106.8	83.5	41.7	65.52	0.36	18
O	850	24.09	0.006	13.73	4.545	84.5	83.2	44.9	66.25	0.36	18
P	870	24.02	0.007	13.6	5.151	72.6	83.3	48.6	66.14	0.32	18
Q	890	24.31	0.0037	14.32	5.764	137	82.6	52.7	66.38	0.3	18
R	910	24.28	0.0041	13.7	7.175	123.1	83.3	57.8	66.89	0.26	18
S	930	24.24	0.0024	13.07	7.985	209.3	84.1	63.5	67.37	0.24	18
T	950	24.67	0.0044	13.72	8.088	115	83.6	69.3	68.14	0.24	18
U	980	25.46	0.0017	14.52	11.509	301.9	83.1	77.5	69.95	0.22	18
V	1010	24.68	0.0013	11.16	18.24	405	86.6	90.5	70.62	0.17	18
W	1040	22.53	0.0021	5.213	13.34	239.4	93.2	100	69.37	0.17	18
Integrated age ± 1σ			n=23		140.2			K2O=9.82%	65.44	0.15	
Plateau ± 1	steps U-W		n=3	MSWD=13.98	43.09			30.7	69.99	0.393	
GR 28, Muscovite, 3.28 mg, J=0.001839±0.07%, D=1.005±0.001, NM-268L, Lab#=63061-01											
A	550	49.37	0.0239	145.7	0.871	21.3	12.8	0.6	21.2	1.9	18
B	600	20.38	0.013	41.43	0.89	39.2	39.9	1.2	27.2	1.6	18
C	650	15.99	0.0028	28.17	1.71	180.2	47.9	2.3	25.6	0.84	18
D	700	17.23	0.0008	33.18	3.382	600.5	43.1	4.6	24.79	0.48	18
E	720	13.85	0.0021	21.08	2.521	238.7	55	6.3	25.45	0.57	18
F	750	13.24	0.0011	19.17	4.778	483.3	57.2	9.5	25.31	0.33	18
G	770	12.76	-0.0005	17.17	6.774	-	60.2	14	25.69	0.26	18
H	775	11.08	0.0006	11.91	6.343	818.7	68.2	18.3	25.25	0.24	18
I	785	12.18	0.0015	15.51	6.467	345.7	62.4	22.6	25.38	0.25	18
J	790	10.18	0.0008	8.899	5.968	645.3	74.2	26.6	25.23	0.25	18
K	800	10.07	0.0003	8.443	6.878	1765	75.2	31.2	25.31	0.21	18
L	820	9.782	0.0002	7.211	9.053	2310	78.2	37.3	25.56	0.17	18
M	850	9.399	0.001	5.94	12.97	498.1	81.3	46	25.53	0.12	18
N	870	9.646	-0.0002	6.83	8.88	-	79.1	51.9	25.48	0.17	18
O	890	10.24	0.0013	8.925	7.269	380.8	74.2	56.8	25.39	0.21	18
P	905	10.98	0.0008	11.58	5.479	672.7	68.8	60.5	25.26	0.27	18

Q	910	11.5	0.0022	13.68	4.385	236.9	64.8	63.4	24.93	0.34	18
R	930	11.44	0.0004	13	4.686	1231	66.4	66.5	25.38	0.32	18
S	950	11.34	0.0018	12.4	4.953	287.2	67.7	69.9	25.63	0.31	18
T	980	11.26	0.0012	11.9	6.514	428.5	68.8	74.2	25.85	0.24	18
U	1010	11.8	-0.0001	13.76	9.469	-	65.5	80.6	25.83	0.19	18
V	1040	10.01	0.0001	7.561	15.93	4920	77.7	91.2	25.96	0.11	18
W	1070	8.367	0.0014	2.083	9.274	366.2	92.6	97.4	25.89	0.15	18
X	1110	8.581	0.0001	3.031	3.322	7126	89.6	99.7	25.67	0.4	18
Y	1140	11.39	0.0048	13.02	0.496	105.3	66.2	100	25.2	2.7	18
Integrated age ± 1σ			n=25		149.3			K2O=9.51%	25.523	0.088	
Plateau ± 1		steps A-Y	n=25	MSWD=1.73	149.3			100	25.592	0.063	

Notes:

Isotopic ratios corrected for blank, radioactive decay, and mass discrimination, not corrected for interfering reactions.

Errors quoted for individual analyses include analytical error only, without interfering reaction or J uncertainties.

Integrated age calculated by summing isotopic measurements of all steps.

Integrated age error calculated by quadratically combining errors of isotopic measurements of all steps.

Plateau age is inverse-variance-weighted mean of selected steps.

Plateau age error is inverse-variance-weighted mean error (Taylor, 1982) times root MSWD where MSWD>1.

Plateau error is weighted error of Taylor (1982).

isotopic abundances after Steiger and Jäger (1977).

x preceding sample ID denotes analyses excluded from plateau age calculations.

D = 1 AMU mass discrimination in favor of light isotopes.

- = No detectable ^{37}Ar above blank levels

Weight percent K_2O calculated from ^{39}Ar signal, sample weight, and instrument sensitivity.

Ages calculated relative to FC-2 Fish Canyon Tuff sanidine interlaboratory standard at 28.201 Ma (Kuiper et al., 2008)

Decay Constant (LambdaK (total)) = 5.463e-10/a (Min et al., 2000)

Correction factors:

$(^{39}Ar/^{37}Ar)_{Ca}$ = 0.0006601 ± 3e-06

$(^{36}Ar/^{37}Ar)_{Ca}$ = 0.0002649 ± 0.0000005

$(^{40}Ar/^{39}Ar)_{K}$ = 0.00601 ± 0.00038

Figure S4. $^{40}Ar/^{39}Ar$ age spectra plots for the Irwin Canyon granite samples.

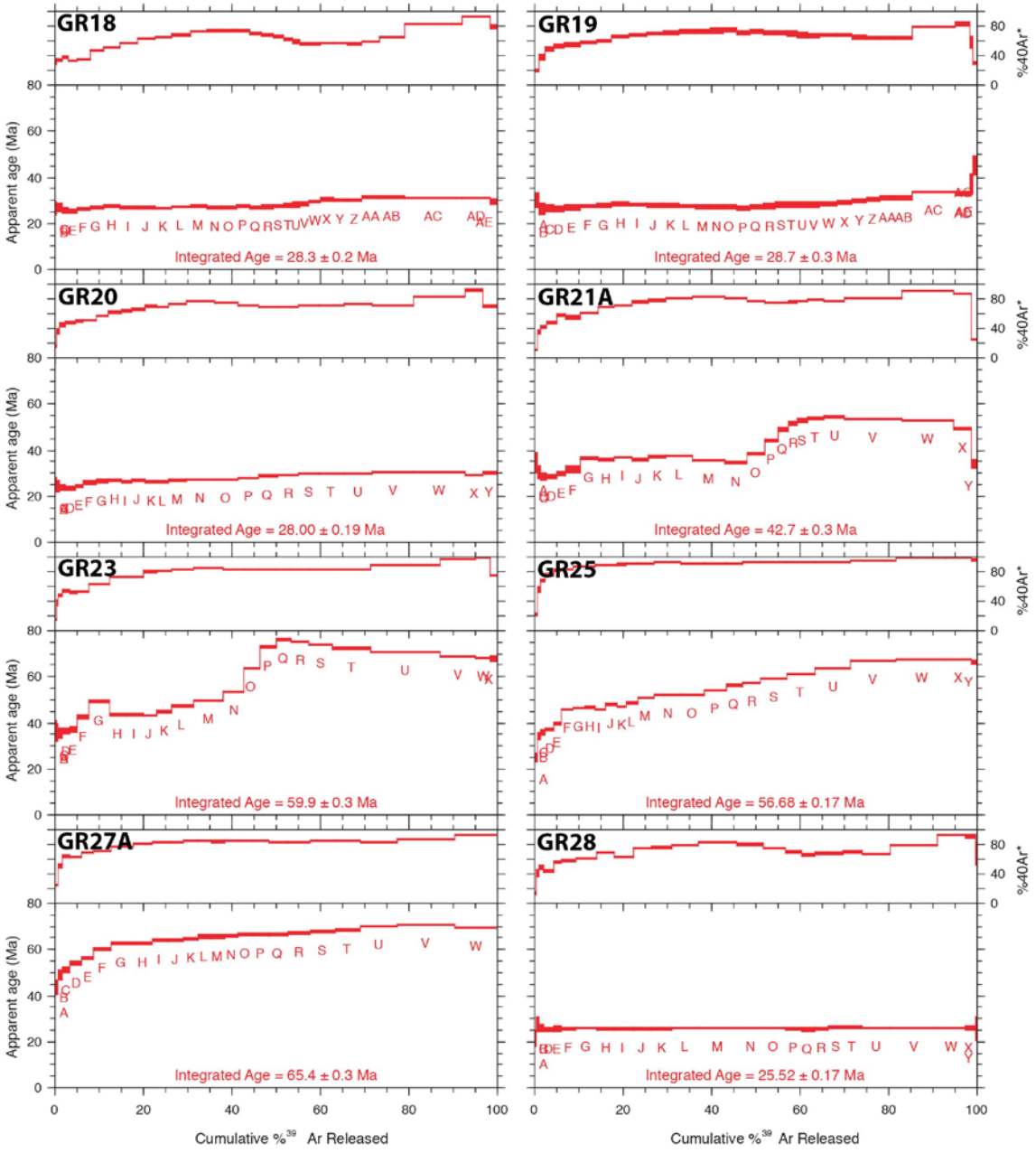

Thermal histories were obtained using a multi-diffusion domain (MDD) model that follows the basic procedures of Lovera et al. (1989) and Sanders et al. (2006). Diffusion coefficients were calculated based on the fractional release of ^{39}Ar and plotted on Arrhenius plots. Log(r/r_0) plots were obtained using an activation energy of 64 kcal/mol (Harrison et al., 2009) and using the convention of placing the reference Arrhenius law to pass through the first heating step such that the log(r/r_o) value is zero for the first increment of gas release. The log(r/r_o) plots are consistent with a multi-domain behavior, with inflections that closely correlate to inflections in the age spectra. The Arrhenius data were forward modeled with an activation energy for each domain of 64 kcal/mol, and a domain distribution that utilizes 5 or 6 domains provides model fits that closely match the measured data. Thermal histories were derived by fitting the measured age spectrum with acceptable fits determined by a Chebyshev's approximation. A minimum of 20 successful model fits was used to determine a mean and 90% confidence interval for the thermal histories. In most cases, the model age spectra closely approximate the measured spectra and return thermal histories that constrain the temperature paths between ~375-425 °C and ~250 °C for the age range provided by the age spectra. Sample GR23 was not modeled as the last 50% of the age spectrum exhibited overall declining ages and is not a form predicted by the MDD model. However, the other 7 samples exhibit remarkable consistency between age spectra and kinetic data and yield robust thermal histories. Kinetic data are provided in Table S5.

Table S5. MDD kinetic parameters for muscovite diffusion domain modeling.

Sample	**GR18**	**GR19**	**GR20**	**GR21A**	**GR23**	**GR25**	**GR28**
Number of domains	5	5	6	6	6	5	6
$\log(D/r_1^2)$ /sec	12.4	12.505	12.052	12.284	11.2	12.5	12.1
volume fraction r_1	0.01	0.027	0.02	0.02	0.02	0.02	0.02
$\log(D/r_2^2)$ /sec	9.249	9.895	9.452	9.284	9.202	10.413	8.964
volume fraction r_2	0.403	0.024	0.078	0.022	0.054	0.03	0.07
$\log(D/r_3^2)$ /sec	7.016	9.247	8.667	8.943	8.828	9.07	8.844
volume fraction r_3	0.137	0.247	0.231	0.227	0.3	0.286	0.365
$\log(D/r_4^2)$ /sec	7.087	8.472	8.231	8.804	6.965	7.318	8.028
volume fraction r_4	0.14	0.261	0.077	0.187	0.145	0.062	0.054
$\log(D/r_5^2)$ /sec	6.871	7.098	6.936	6.663	6.961	7.301	6.985
volume fraction r_5	0.31	0.441	0.166	0.252	0.281	0.602	0.233
$\log(D/r_6^2)$ /sec			6.816	6.642	6.897		6.982
volume fraction r_6			0.428	0.292	0.2		0.258
E (kcal/mol)	64	64	64	64	64	64	64
$\log(D_o/r_o^2)$ /sec	9.5	10	9.6	9.4	9.2	9.7	9.3

Figure S5 (following 4 pages). Supporting graphs for muscovite $^{40}Ar/^{39}Ar$ MDD modeling. For each model, measured data are shown in blue and model outputs are shown in red.

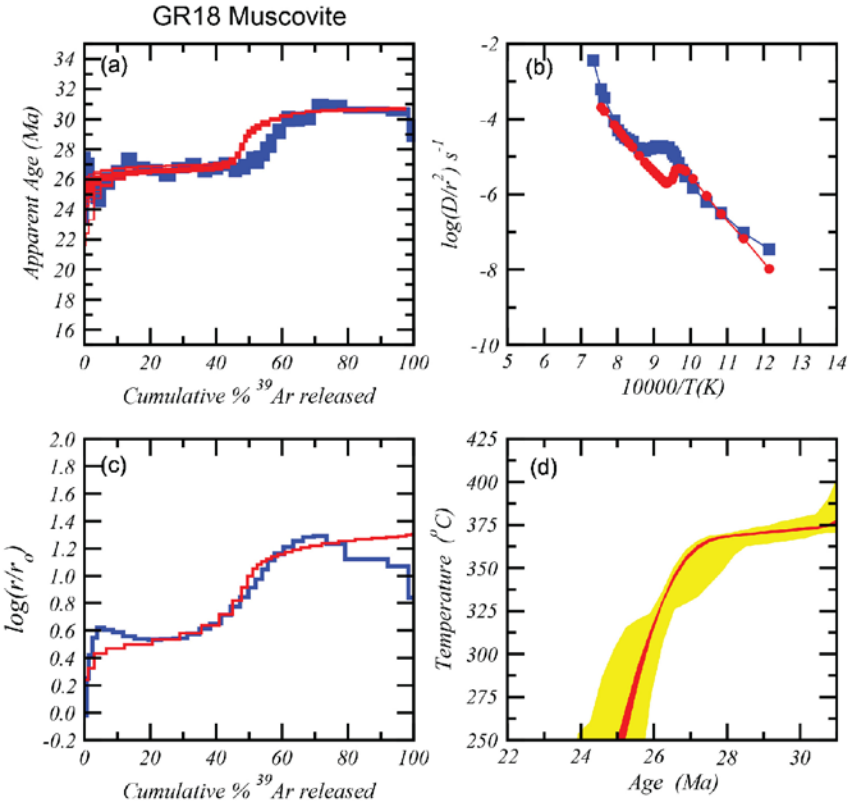
GR18 Muscovite
(a)
Apparent Age (Ma)
Cumulative % 39Ar released
(b)
log(D/r2) s-1
10000/T(K)
(c)
log(r/ro)
Cumulative % 39Ar released
(d)
Temperature (°C)
Age (Ma)

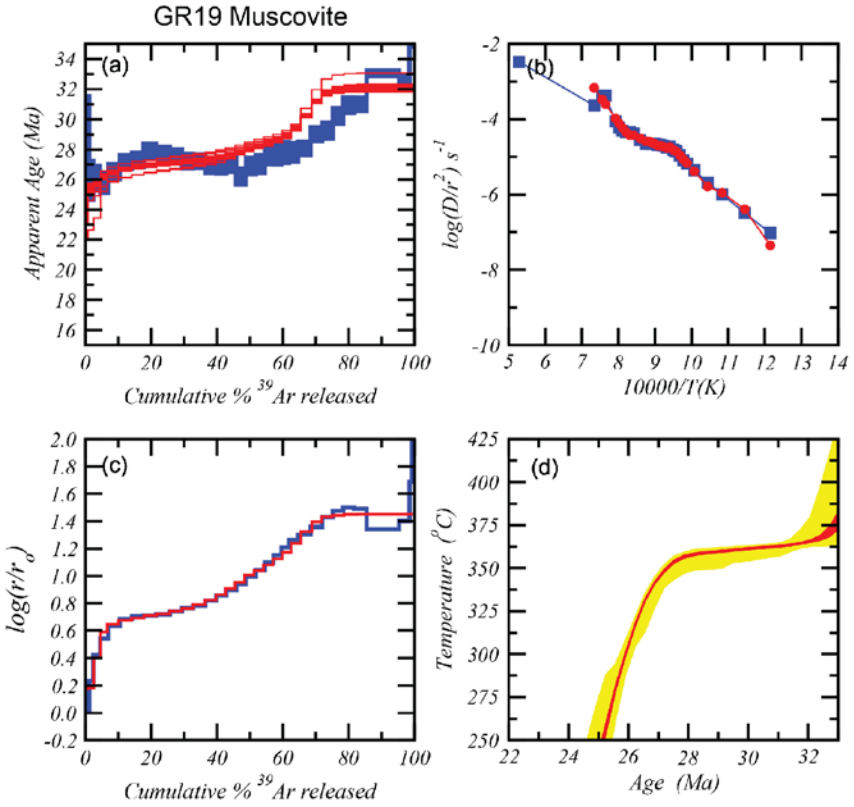
GR19 Muscovite
(a)
Apparent Age (Ma)
Cumulative % 39Ar released
(b)
log(D/r2) s-1
10000/T(K)
(c)
log(r/ro)
Cumulative % 39Ar released
(d)
Temperature (°C)
Age (Ma)

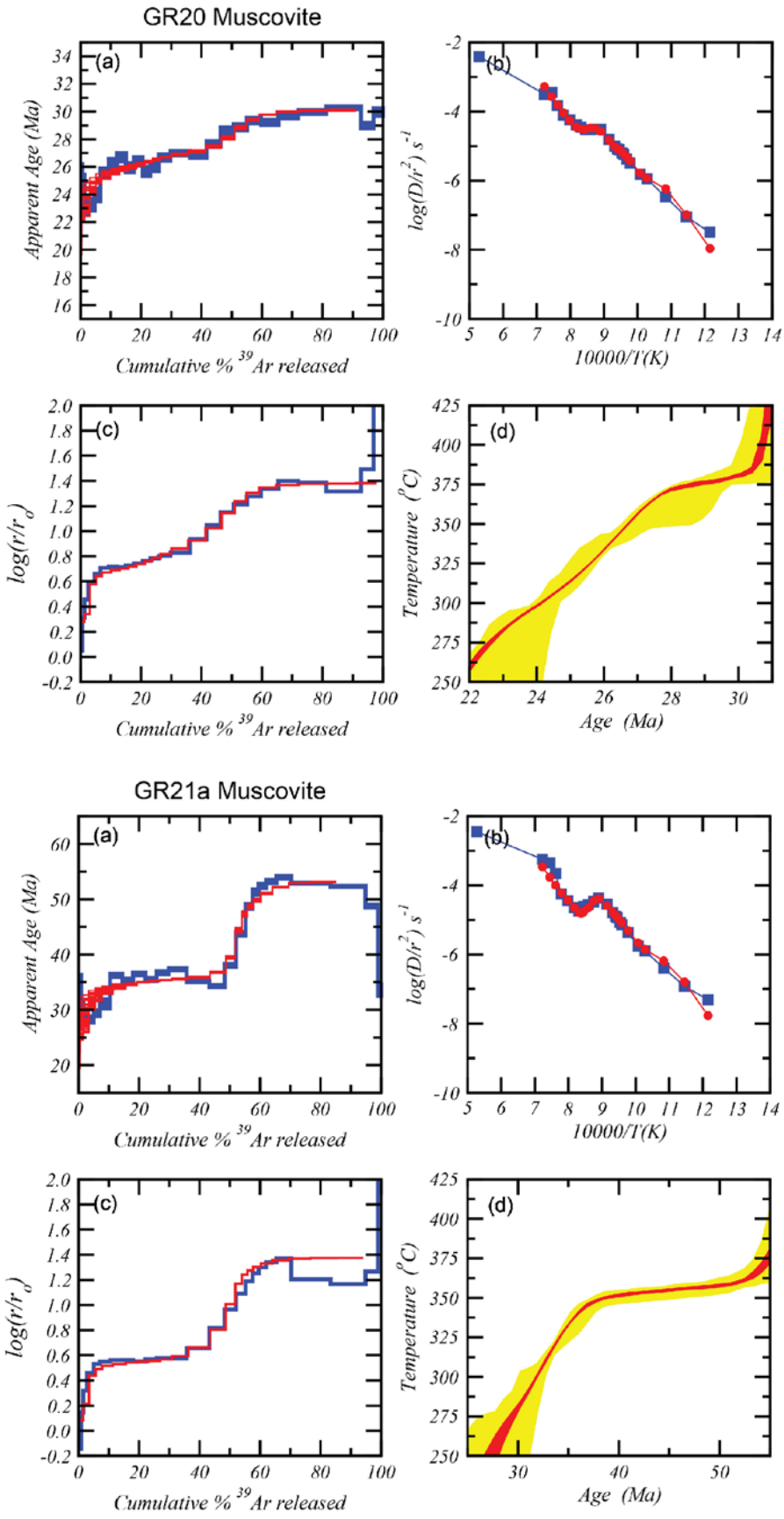
GR20 Muscovite
(a)
Apparent Age (Ma)
Cumulative % 39Ar released
(b)
log(D/r2) s-1
10000/T(K)
(c)
log(r/ro)
Cumulative % 39Ar released
(d)
Temperature (°C)
Age (Ma)
GR21a Muscovite
(a)
Apparent Age (Ma)
Cumulative % 39Ar released
(b)
log(D/r2) s-1
10000/T(K)
(c)
log(r/ro)
Cumulative % 39Ar released
(d)
Temperature (°C)
Age (Ma)

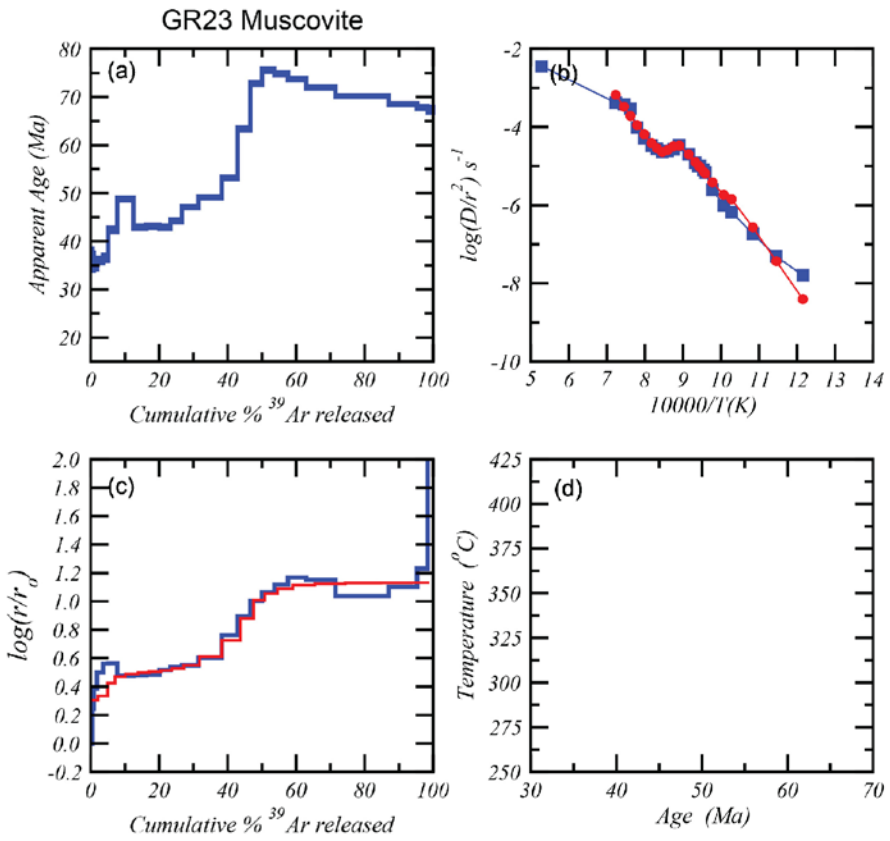
GR23 Muscovite
(a)
Apparent Age (Ma)
Cumulative % 39Ar released
(b)
log(D/r2) s-1
10000/T(K)
(c)
log(r/ro)
Cumulative % 39Ar released
(d)
Temperature (°C)
Age (Ma)

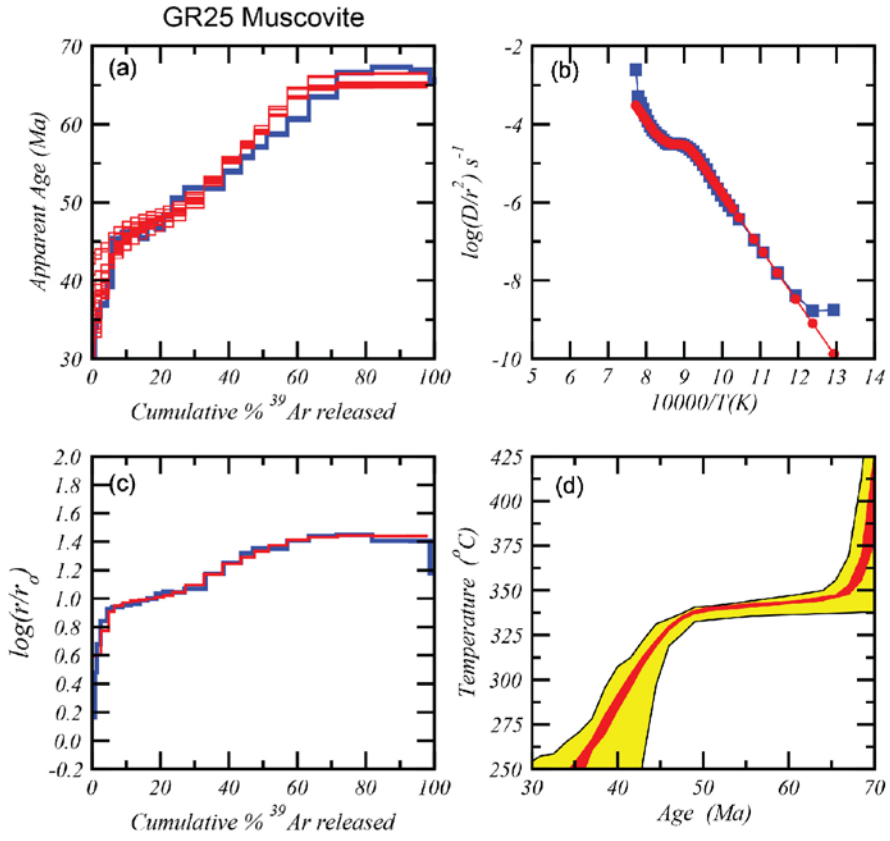
GR25 Muscovite
(a)
Apparent Age (Ma)
Cumulative % 39Ar released
(b)
log(D/r2) s-1
10000/T(K)
(c)
log(r/ro)
Cumulative % 39Ar released
(d)
Temperature (°C)
Age (Ma)

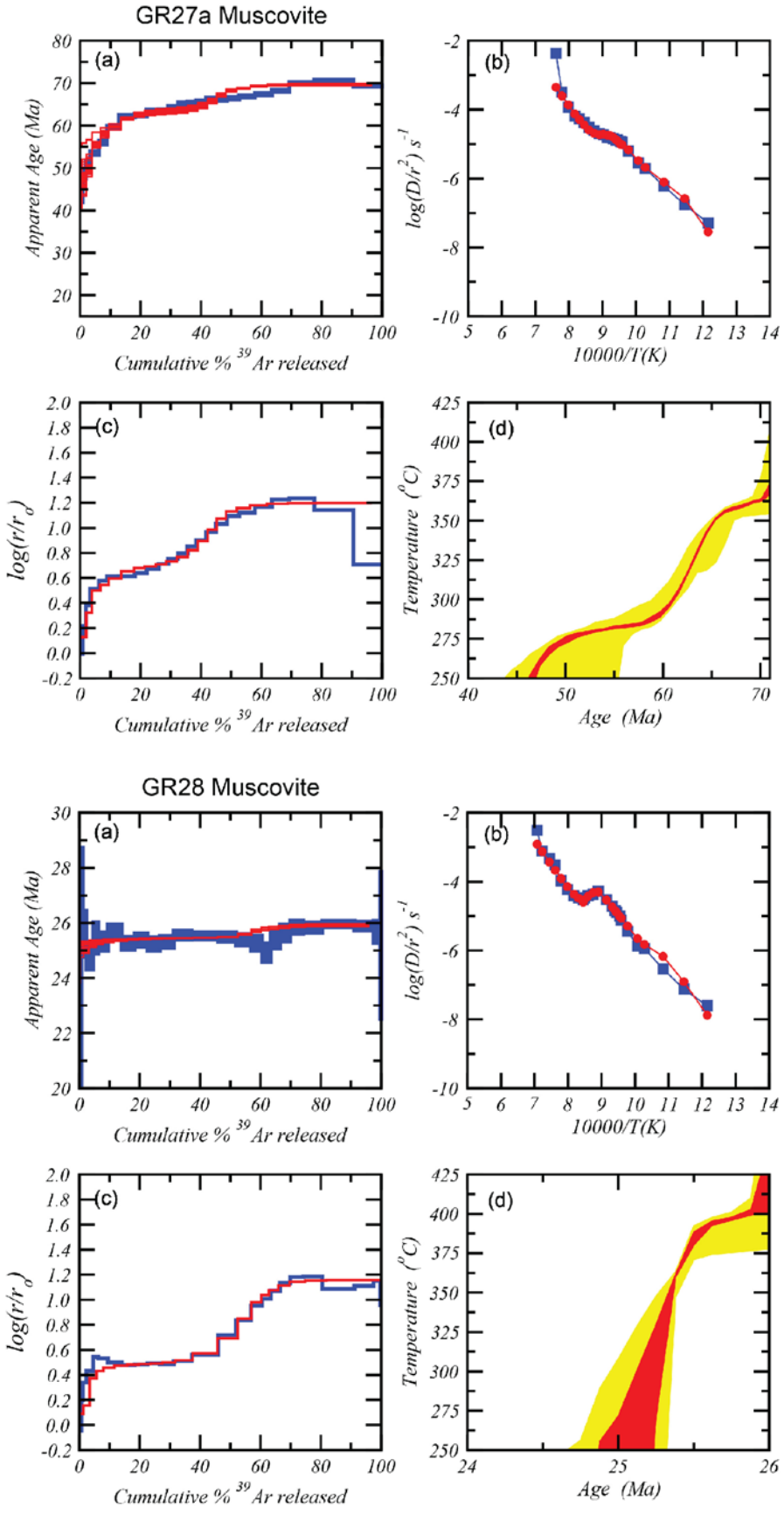
GR27a Muscovite
(a)
Apparent Age (Ma)
Cumulative % 39Ar released
(b)
log(D/r2) s-1
10000/T(K)
(c)
log(r/ro)
Cumulative % 39Ar released
(d)
Temperature (°C)
Age (Ma)
GR28 Muscovite
(a)
Apparent Age (Ma)
Cumulative % 39Ar released
(b)
log(D/r2) s-1
10000/T(K)
(c)
log(r/ro)
Cumulative % 39Ar released
(d)
Temperature (°C)
Age (Ma)

Text S8. Methodology and supporting data for zircon and apatite fission track ages

Analyses on zircon and apatite separated from Grant Range granite samples were performed at the University of Arizona Fission-Track Lab by S. Thomson. Supporting data are shown in Table S6 (single-grain data tables for individual samples are available upon request from the corresponding author). Apatite grains were mounted in epoxy resin, alumina and diamond polished, and spontaneous fission tracks were revealed by etching with 5.5M HNO_3 at 20°C for 20 seconds. Zircon grains were mounted in PFA Teflon, diamond polished, and etched in an oven at ca. 220 °C using a KOH-NaOH eutectic melt (Gleadow et al., 1976) in a zirconium crucible for 3 to 50+ hours. The optimum etch time is dependent on age and radiation damage, and was monitored by repeated etching and observation at 3-6 hour time intervals. Samples were analyzed by applying the external detector method (Gleadow, 1981) using very low uranium, annealed muscovite mica detectors, and irradiated at the Oregon State University Triga Reactor, Corvallis, U.S.A. The neutron fluence was monitored using European Institute for Reference Materials and Measurements (IRMM) uranium-dosed glasses IRMM 540R for apatite and IRMM 541 for zircon. After irradiation, induced tracks in the mica external detectors were revealed by etching with 48% HF for 18 minutes. Spontaneous and induced fission track densities were counted using an Olympus BX61 microscope at 1250x magnification with an automated Kinetek Stage system. Apatite fission track lengths and Dpar values were measured using FTStage software, and an attached drawing tube and digitizing tablet supplied by T. Dumitru of Stanford University calibrated against a stage micrometer. Central ages (Galbraith and Laslett, 1993; Galbraith, 2005), quoted with 1σ errors, are calculated using the IUGS recommended zeta-calibration approach of Hurford and Green (1983). Current apatite and zircon IRMM 540R and IRMM541 zeta calibration factors of 368.1 ± 14.9 and 121.3 ± 2.6, respectively, have been obtained by repeated calibration against a number of internationally-agreed age standards including Durango and Fish Canyon apatite, and Fish Canyon and Buluk zircon, according to the recommendations of Hurford (1990).

Table S6. Supporting data for zircon and apatite fission track analyses of the Irwin Canyon granite samples.

Sample No.	Mineral	No. of Crystals	Track Density (x 10^6 tr cm^{-2})			Age Dispersion	Central Age (Ma) (±1σ)
			ρs (N_s)	ρi (N_i)	ρd (N_d)	($P\chi^2$)	
GR19	Apatite	20	0.1098 (119)	1.433 (1553)	1.217 (3894)	<0.01% (99.9%)	**17.1±1.8**
	Zircon	20	5.187 (1215)	4.653 (1090)	0.3544 (2268)	<0.01% (99.8%)	**23.9±1.3**
GR18	Apatite	18	0.1091 (88)	1.374 (1108)	1.208 (3866)	<0.01% (98.2%)	**17.6±2.1**
	Zircon	15	2.865 (651)	2.614 (594)	0.3534 (2262)	<0.01% (99.8%)	**23.4±1.6**
GR20	Apatite	20	0.0923 (74)	1.085 (870)	1.198 (3837)	<0.01% (99.8%)	**18.7±2.4**
	Zircon	5	9.766 (175)	9.152 (164)	0.3523 (2255)	<0.01% (99.5%)	**22.7±2.6**
GR21A	Apatite	20	0.0646 (66)	0.8033 (821)	1.190 (3809)	<0.01% (>99.9%)	**17.6±2.4**
	Zircon	20	3.963 (2303)	3.509 (2039)	0.3513 (2248)	<0.01% (99.9%)	**24.0±1.1**
GR23	Apatite	20	0.1161 (90)	1.332 (1032)	1.181 (3781)	<0.01% (>99.9%)	**18.9±2.2**
	Zircon	9	4.195 (792)	3.040 (574)	0.3502 (2242)	0.25% (52.6%)	**29.2±1.9**
GR25	Apatite	20	0.0763 (49)	0.8746 (562)	1.173 (3752)	<0.01% (99.9%)	**18.8±2.9**
	Zircon	8	4.024 (613)	3.453 (526)	0.3492 (2235)	<0.01% (96.1%)	**24.6±1.7**
GR27A	Apatite	20	0.1233 (83)	1.527 (1028)	1.155 (3698)	<0.01% (>99.9%)	**17.1±2.1**
	Zircon	14	6.381 (1654)	5.424 (1406)	0.3482 (2228)	<0.01% (97.9%)	**24.8±1.3**
GR28	Apatite	20	0.1223 (115)	1.588 (1493)	1.146 (3667)	<0.01% (99.9%)	**16.2±1.7**
	Zircon	16	4.254 (1304)	4.117 (1262)	0.3471 (2222)	<0.01% (98.1%)	**21.7±1.2**

Notes:
(i). Analyses by external detector method using 0.5 for the $4\pi/2\pi$ geometry correction factor;
(ii). Ages calculated using dosimeter glass: IRMM540R with ζ_{540R} = 368.1±14.9 (apatite); IRMM541 with ζ_{541} = 121.1±3.5 (zircon);
(iii). $P\chi^2$ is the probability of obtaining a χ^2 value for v degrees of freedom where v = no. of crystals - 1

Text S9. Methodology and supporting data for zircon and apatite (U-Th)/He ages.

(U-Th)/He dating of zircon and apatite separated from the Irwin Canyon granite samples was performed at the University of Arizona Radiogenic Helium Dating Laboratory. Analyses followed the procedures outlined in Reiners et al. (2004) and Reiners (2005). Individual grains were selected from separates on the basis of size, morphology, and lack of inclusions. Grains lacking obvious fractures and with a minimum radius of 60 μm, with

minimal to no inclusions, were selected. The dimensions of individual grains were measured from digital photomicrographs, using the approach outlined in Hourigan et al. (2005) for alpha-ejection corrections. Single grains were then packed into 1-mm Nb foil envelopes. Multiple foil packets were then placed in individual holes in a 30-hole planchett inside a ~7-cm laser cell pumped to <10-9 torr. For zircon, individual packets were then heated for 15 minutes by a focused beam of a 1-2 W laser, to extract ^{4}He. The packets were then re-heated for 15 minutes, often multiple times, until ^{4}He yields were less than 1% of total. For apatite, the procedure was similar, except the packets were heated for 3 minutes during the first extract and all following re-extracts. For zircon analyses, standards of Fish Canyon Tuff zircon (28.48 ± 0.06 Ma (2σ), Schmitz and Bowring, 2001) were analyzed between every 5 unknowns. For apatite analyses, standards of Durango apatite (31.44 ± 0.18 Ma (2σ); McDowell et al., 2005) were analyzed between every 5 unknowns.

Gas released from heated samples was spiked with 0.1-0.2 pmol ^{3}He, and condensed onto activated charcoal at the cold head of a cryogenic trap at 16 K. Helium was then released from the cold head at 37 K into a small volume (~50 cc) with an activated Zr-Ti alloy getter and the source of a Balzers quadrupole mass spectrometer (QMS) with a Channeltron electron multiplier. Peak-centered masses at approximately m/z of 1, 3, 4, and 5.2 were measured. Mass 5.2 establishes background, and mass 1 is used to correct mass 3 for HD and H3+. Corrected ratios of masses 4 to 3 were regressed through ten measurement cycles over ~15 seconds to derive an intercept value, which has an uncertainty of 0.05-0.5% over a ^{4}He/^{3}He range of ~103, and compared with the mean corrected ratio to check for significant anomalous changes in the ratio during analysis. Helium contents of unknown samples were calculated by first subtracting the average mass-1-corrected ^{4}He/^{3}He measured on multiple procedural blanks analyzed by the same method, from the mass-1-corrected ^{4}He/^{3}He measured on the unknown. This was then ratioed to the mass-1-corrected ^{4}He/^{3}He measured on a shot of an online reference ^{4}He standard analyzed with the same procedure. The resulting ratio of measured ^{4}He/^{3}He values was then multiplied by the moles of ^{4}He delivered in the reference shot.

After He extraction and measurement, foil packets were retrieved and transferred to Teflon vials. Vials containing zircon were spiked with a 50 ml shot containing 7.55 ± 0.10 ng/ml ^{233}U and 12.3 ± 0.10 ng/ml ^{229}Th, and vials containing apatite were spiked with a 50 ml shot of a 97%-enriched ^{147}Sm spike with 10.8 ± 0.10 ng/ml Sm. High-pressure digestion vessels were used for dissolution of the zircon, apatite, and Nb foil packet. Natural-to-spike isotope ratios of U and Th were then measured on a high-resolution (single-collector) Element2 ICP-MS with all-PFA Teflon sample introduction equipment and sample preparation/analytical equipment. Blanks for zircon analyses were 2.6±0.5 pg U and 5.5±1.0 pg Th.

Precision on measured U-Th ratios is typically better than 0.5% for zircon analyses. Propagated analytical uncertainties for typical zircon samples lead to an estimated analytical uncertainty on (U-Th)/He ages of approximately 1-3% (1σ). In some cases,

reproducibility of multiple aliquots approaches analytical uncertainty. However, in general, reproducibility of repeat analyses of (U-Th)/He ages is significantly worse than analytical precision. Thus (U-Th)/He ages typically show a much greater scatter and higher MSWD than expected based on analytical precision alone, and multiple replicate analyses of (U-Th)/He ages on several aliquots is necessary for confidence in a particular sample age. Single-grain zircon and apatite (U-Th)/He ages and supporting data are shown on Tables S7 and S8, respectively, and weighted mean ages are shown on Table 2 in the text. Single-grain ages are reported with 2σ formal analytical precision, and weighted mean ages are reported with 2σ standard error.

Table S7. Single-grain zircon (U-Th)/He ages and supporting data.

Sample name	pmol He	1σ ± pmol He	ng U	1σ ± ng U	ng Th	1σ ± ng Th	Th/U	raw age (Ma)	2σ ± raw age (Ma)	Ft ^{238}U	Ft ^{235}U	Ft ^{232}Th	half-width (μm)	ppm U (morph)	1σ ± ppm U (morph)	ppm Th (morph)	1σ ± ppm Th (morph)	nmol ^{4}He/g (morph)	1σ ± nmol ^{4}He/g (morph)	corrected age (Ma)	2σ ± corrected age (Ma)
GR18_Zr1	0.25	0.00	5.09	0.07	0.60	0.01	0.12	9.00	0.27	0.82	0.79	0.79	68.09	441.51	6.32	52.28	0.83	22.02	0.13	11.00	0.32
GR18_Zr2	0.54	0.00	10.37	0.15	0.97	0.02	0.10	9.39	0.27	0.81	0.78	0.78	65.38	1044.71	14.91	97.77	1.65	54.03	0.31	11.58	0.34
GR18_Zr3	0.35	0.00	7.47	0.13	0.29	0.01	0.04	8.51	0.30	0.78	0.74	0.74	54.25	1392.42	24.31	54.55	1.12	64.41	0.36	10.97	0.39
weighted mean																				11.19	0.20
GR19_Zr1	0.18	0.00	3.87	0.06	0.15	0.00	0.04	8.79	0.29	0.73	0.69	0.69	43.30	1434.65	22.84	56.31	0.95	68.60	0.44	12.15	0.40
GR19_Zr3	0.84	0.00	15.70	0.26	0.58	0.01	0.04	9.84	0.33	0.80	0.77	0.77	59.64	2062.44	34.18	76.38	1.33	110.39	0.61	12.39	0.42
weighted mean																				12.27	0.29
GR20_Zr1	0.12	0.00	2.43	0.04	0.51	0.01	0.22	8.66	0.29	0.71	0.67	0.67	41.14	771.79	12.80	161.75	2.48	37.82	0.28	12.22	0.41
GR20_Zr3	0.06	0.00	1.62	0.03	0.16	0.00	0.10	6.43	0.23	0.72	0.68	0.68	42.31	665.52	11.28	66.41	1.19	23.62	0.19	8.98	0.32
weighted mean																				10.19	0.25
GR21A_Zr1	0.83	0.00	16.19	0.26	0.65	0.01	0.04	9.47	0.31	0.77	0.74	0.74	53.05	2638.10	41.83	105.97	1.53	135.92	0.80	12.29	0.40
GR21A_Zr2	0.73	0.00	11.74	0.17	1.16	0.02	0.10	11.29	0.33	0.75	0.71	0.71	48.04	1949.90	27.92	193.22	2.80	121.49	0.67	15.10	0.44
GR21A_Zr3	1.04	0.01	19.19	0.31	1.63	0.02	0.09	9.81	0.32	0.77	0.74	0.74	53.34	3070.31	49.60	261.03	3.75	165.68	1.03	12.72	0.42
weighted mean																				13.28	0.24
GR23_Zr1	0.12	0.00	2.79	0.04	0.27	0.00	0.10	7.77	0.23	0.80	0.77	0.77	62.30	332.31	4.76	31.73	0.53	14.24	0.09	9.69	0.29
GR23_Zr2	0.30	0.00	6.42	0.11	0.32	0.01	0.05	8.43	0.28	0.76	0.72	0.72	49.11	1395.76	23.26	70.59	1.10	64.18	0.37	11.19	0.38
GR23_Zr3	0.10	0.00	1.71	0.03	0.42	0.01	0.25	10.34	0.33	0.78	0.74	0.74	54.06	268.22	4.37	65.52	1.02	15.81	0.09	13.37	0.43
weighted mean																				10.96	0.20
GR25_Zr1	0.11	0.00	2.21	0.03	0.32	0.00	0.15	9.27	0.26	0.79	0.76	0.76	58.60	307.77	4.40	45.05	0.65	15.90	0.08	11.72	0.33
GR25_Zr2	0.35	0.00	6.53	0.12	0.51	0.01	0.08	9.90	0.35	0.80	0.77	0.77	61.68	765.61	13.92	59.34	0.98	41.58	0.18	12.36	0.44
GR25_Zr3	0.14	0.00	2.85	0.05	0.32	0.01	0.12	9.04	0.29	0.78	0.75	0.75	56.12	488.46	7.89	54.85	0.93	24.44	0.14	11.57	0.37
weighted mean																				11.83	0.22
GR27A_Zr1	0.06	0.00	1.09	0.02	0.22	0.00	0.21	9.85	0.32	0.65	0.61	0.61	33.62	635.98	10.15	128.47	1.85	35.38	0.24	15.13	0.49
GR27A_Zr2	0.21	0.00	2.70	0.04	0.17	0.00	0.07	14.03	0.40	0.67	0.62	0.62	34.87	1622.92	23.34	104.68	1.59	124.60	0.55	21.13	0.61
weighted mean																				17.51	0.38
GR28_Zr1	0.44	0.00	8.83	0.13	1.33	0.02	0.15	8.93	0.25	0.77	0.74	0.74	53.17	1489.25	21.28	223.73	3.24	74.26	0.33	11.60	0.33
GR28_Zr2	1.31	0.01	24.73	0.35	1.43	0.02	0.06	9.66	0.28	0.88	0.87	0.87	108.15	615.39	8.82	35.60	0.51	32.48	0.14	10.94	0.31
GR28_Zr3	0.40	0.00	6.48	0.09	0.43	0.01	0.07	11.17	0.32	0.74	0.70	0.70	45.55	1914.50	27.31	126.29	1.84	117.04	0.61	15.18	0.44
weighted mean																				12.07	0.20

Notes:

1. Ft is alpha ejection correction (Reiners, 2005).
2. Singe-grain ages are reported with 2σ formal analytical precision.
3. Weighted mean ages are reported with 2σ standard error, calculated from Isoplot, version 4.1 (Ludwig, 2008).
4. Half-width is c-axis perpendicular half-width.

Table S8. Single-grain apatite (U-Th)/He ages and supporting data.

Sample name	pmol He	1σ ± pmol He	ng U	1σ ± ng U	ng Th	1σ ± ng Th	Th/U	raw age (Ma)	2σ ± raw age (Ma)	Ft ^{238}U	Ft ^{235}U	Ft ^{232}Th	Ft ^{147}Sm	half-width (μm)	ppm U (mcrph)	1σ ± ppm U (morph)	ppm Th (morph)	1σ ± ppm Th (morph)	nmol ^{4}He/g (morph)	1σ ± nmol ^{4}He/g (morph)	corrected age (Ma)	2σ ± corrected age (Ma)
GR18_Ap1	0.00	0.00	0.07	0.00	0.01	0.00	0.18	9.48	0.40	0.79	0.76	0.76	0.93	70.02	8.81	0.13	1.51	0.03	0.48	0.01	11.96	0.51
GR18_Ap2	0.05	0.00	0.16	0.00	1.09	0.02	6.87	20.03	0.47	0.80	0.77	0.77	0.94	72.33	16.40	0.23	109.88	1.64	4.60	0.02	25.62	0.59
GR18_Ap3	0.00	0.00	0.05	0.00	0.02	0.00	0.47	16.82	0.65	0.83	0.80	0.80	0.94	84.35	3.42	0.05	1.55	0.05	0.35	0.01	20.35	0.79
weighted mean																					18.23	0.35
GR20_Ap1	0.00	0.00	0.03	0.00	0.01	0.00	0.19	10.21	0.47	0.71	0.67	0.67	0.91	48.07	13.06	0.19	2.44	0.08	0.76	0.01	14.46	0.67
GR20_Ap2	0.00	0.00	0.03	0.00	0.00	0.00	0.12	12.71	0.53	0.67	0.62	0.62	0.89	41.60	14.16	0.21	1.65	0.06	1.01	0.02	19.11	0.80
GR20_Ap3	0.00	0.00	0.04	0.00	0.01	0.00	0.15	9.57	0.55	0.74	0.71	0.71	0.92	55.87	8.84	0.13	1.28	0.04	0.48	0.01	12.85	0.73
weighted mean																					15.22	0.42
GR21A_Ap2	0.00	0.00	0.02	0.00	0.01	0.00	0.35	15.07	0.56	0.70	0.66	0.66	0.90	46.26	9.62	0.14	3.26	0.07	0.85	0.01	21.73	0.81
GR21A_Ap3	0.00	0.00	0.02	0.00	0.00	0.00	0.24	9.76	1.30	0.67	0.63	0.63	0.89	42.55	9.25	0.14	2.15	0.07	0.52	0.03	14.57	1.94
weighted mean																					20.66	0.75
GR23_Ap1	0.01	0.00	0.08	0.00	0.02	0.00	0.32	13.99	0.48	0.78	0.75	0.75	0.93	65.87	11.26	0.17	3.56	0.06	0.93	0.01	17.94	0.61
GR23_Ap3	0.01	0.00	0.06	0.00	0.06	0.00	1.10	16.95	0.59	0.73	0.69	0.69	0.91	52.21	15.48	0.22	16.61	0.25	1.79	0.02	23.52	0.82
weighted mean																					19.92	0.49
GR25_Ap1	0.00	0.00	0.02	0.00	0.00	0.00	0.14	16.08	0.81	0.64	0.59	0.59	0.88	37.96	15.77	0.23	2.17	0.10	1.43	0.03	25.26	1.27
GR25_Ap2	0.00	0.00	0.01	0.00	0.00	0.00	0.28	7.71	0.79	0.65	0.60	0.60	0.88	39.07	6.91	0.12	1.92	0.10	0.31	0.02	11.93	1.22
weighted mean																					18.32	0.88
GR27A_Ap1	0.00	0.00	0.03	0.00	0.01	0.00	0.52	10.63	0.69	0.77	0.73	0.73	0.92	61.27	6.46	0.10	3.31	0.06	0.42	0.01	13.92	0.91
GR27A_Ap2	0.00	0.00	0.02	0.00	0.01	0.00	0.50	8.72	1.48	0.63	0.58	0.58	0.88	36.77	13.50	0.21	6.56	0.17	0.71	0.06	14.02	2.38
GR27A_Ap3	0.00	0.00	0.01	0.00	0.01	0.00	0.41	8.39	0.78	0.67	0.63	0.63	0.89	42.89	7.31	0.12	2.89	0.08	0.37	0.02	12.45	1.15
weighted mean																					13.41	0.68
GR28_Ap1	0.00	0.00	0.06	0.00	0.01	0.00	0.15	10.34	0.39	0.79	0.76	0.76	0.93	67.67	7.85	0.11	1.17	0.03	0.46	0.01	13.15	0.49
GR28_Ap2	0.00	0.00	0.04	0.00	0.01	0.00	0.13	8.66	0.55	0.76	0.73	0.73	0.92	61.20	7.88	0.11	0.97	0.03	0.38	0.01	11.32	0.71
weighted mean																					12.57	0.40

Notes:

1. Ft is alpha ejection correction (Reiners, 2005).
2. Singe-grain ages are reported with 2σ formal analytical precision.
3. Weighted mean ages are reported with 2σ standard error, calculated from isoplot, version 4.1 (Ludwig, 2008).
4. Half-width is c-axis perpendicular half-width.

Text S10. Supporting data for U zonation in the analyzed zircons.

The weighted mean ZHe ages for seven of the eight granite samples (all but sample GR27A) are typically between 4 and 8 Myr younger than the AFT and AHe ages from the corresponding samples (Table 2 in the main text). This inversion is interpreted as the result of zonation in the zircons that resulted in U-enriched rims and tips, which led to anomalously high alpha ejection (e.g., Hourigan et al., 2005; Orme et al., 2015). This interpretation is supported by photomicrographs of the zircon grains and mica external detectors that were utilized to collect the ZFT ages from these samples, which exhibit a high concentration of natural and induced fission tracks within the rims, and a paucity of tracks in the grain centers (Fig. S6). Zonation in the zircons is also supported by a positive age-eU correlation (Fig. S7A), and low Th/U values (typically ~0.05-0.15) that are consistent with overgrowth of Th-poor metamorphic rims (e.g., Orme et al., 2015) (Fig. S7B). In light of this evidence for zonation, and the consistency within and between the AFT and AHe datasets, the inverted ZHe ages for these seven samples are not interpreted to be representative of the timing of exhumation-related cooling.

Figure S6. Representative photomicrographs of zircon grains and mica detectors used in collection of ZFT data, which show a concentration of natural and induced fission tracks in the rims.

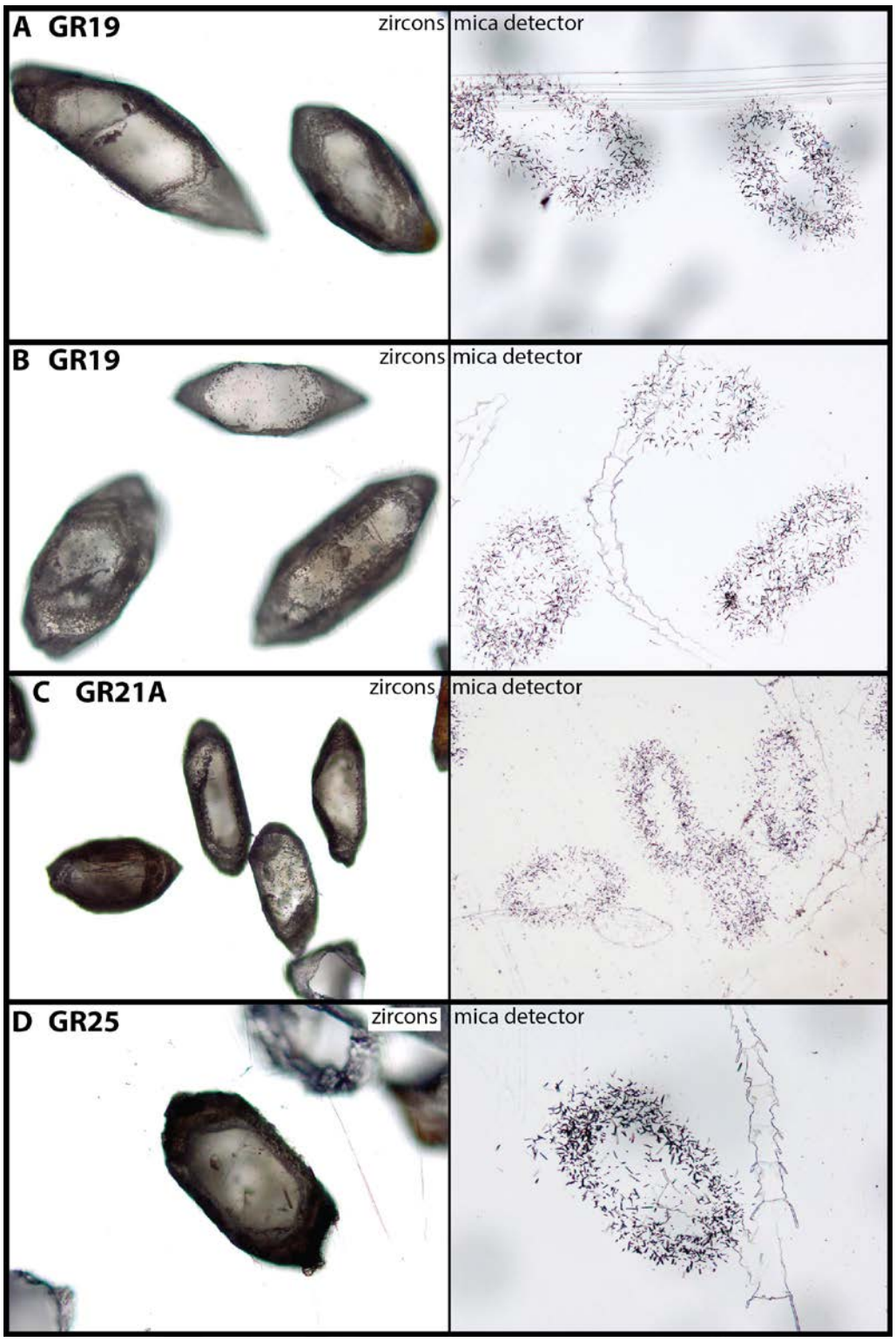

Figure S7. Graphs of (A) age versus eU and (B) age versus Th/U for the zircon (U-Th)/He single-grain analyses. The slight positive correlation on the age-eU graph is consistent with U zonation, and the overall low Th/U values (typically ~0.05-0.15) is consistent with overgrowth of Th-poor metamorphic rims.

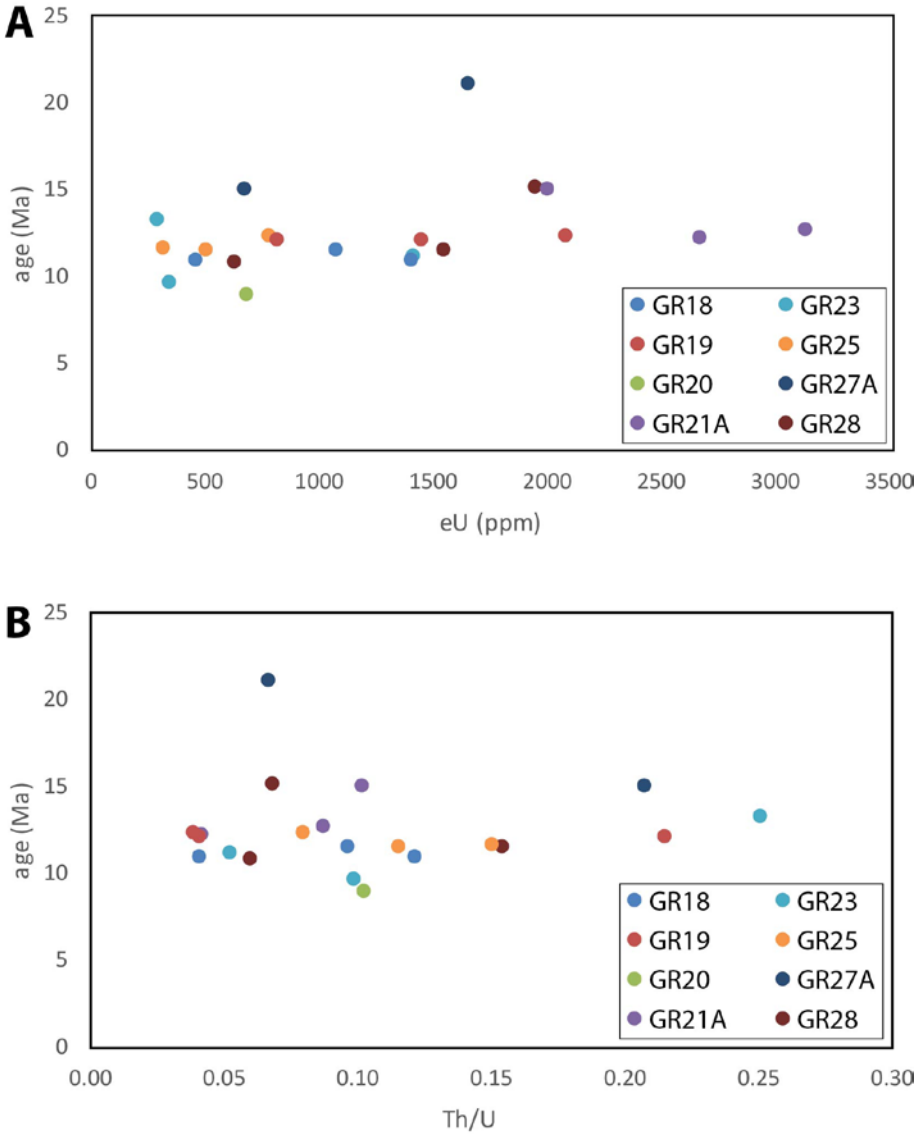

Text S11. Supporting information for HeFTy temperature-time (T-t) path modeling

(U-Th)/He and fission track ages were input into HeFTy version 1.9.1 (Ketcham, 2005) in order to inverse-model T-t paths for the eight Irwin Canyon granite samples. The following section describes methodology and modeling parameters.

For the ZHe model: Calibration: "Guenthner et al., 2013 (Zircon)"; Radius: Average radius of all grains used to calculate the sample weighted mean age (from the 'half-width (μm)' column on Table S6); Abraded: "0 μm" (default); Model precision: "Good"; Stopping distances: "Ketcham et al. 2011"; Alpha calculation: "Ejection"; Measured age (uncorrected): The weighted mean (U-Th)/He age of uncorrected ages (from the 'raw age' column on Table S6 and associated 1σ error) was input here, so that the resulting corrected age is equivalent to the corrected weighted mean age for the sample; Age to report: "Corrected"; Alpha correction: "Ketcham et al. 2011"; Composition: The average U and Th concentration of all grains used to calculate the weighted mean age of the sample (from the 'ppm U' and 'ppm Th' column on Table S6) was input here; Zoned? "No."

For the AFT model: Annealing model: "Ketcham et al. (2007a)"; C-axis projection: "Ketcham et al. (2007b), 5.0M"; Model C axis projected lengths?: "No"; Used Cf Irradiation?: "No"; Default initial mean track length: "From Dpar (μm), 16.3 μm" (default); Length reduction in standard: "0.893" (default); Kinetic parameter: "Dpar (μm)." Each sample was modeled using a single kinetic parameter (Dpar (μm)). Zeta mode: "Traditional"; Uncertainty mode: "1 SE."

For the AHe model: Calibration: "Shuster et al. (2006) (Do/a2) (Apatite)"; Radius: Average radius of all grains used to calculate the sample weighted mean age (from the 'half-width (μm)' column on Table S7); Abraded: "0 μm" (default); Model precision: "Good"; Stopping distances: "Ketcham et al. 2011"; Alpha calculation: "Static ejection"; Measured age (uncorrected): The weighted mean (U-Th)/He age of uncorrected ages (from the 'raw age' column on Table S7 and associated 1σ error) was input here, so that the resulting corrected age is equivalent to the corrected weighted mean age for the sample; Age to report: "Corrected"; Alpha correction: "Ketcham et al. 2011"; Composition: The average U and Th concentration of all grains used to calculate the weighted mean age of the sample (from the 'ppm U' and 'ppm Th' columns on Table S7) was input here; Zoned? "No."

For ZFT data, the calibration options available in HeFTy correspond to predicted closure temperatures (at a cooling rate of 10°C/Myr) between ~280-325˚C, which are characteristic of zircons with zero radiation damage (Rahn et al., 2004; Yamada et al., 2007). Therefore, because this study analyzed zircons from Jurassic-Cretaceous granite, which must have some degree of radiation damage, ZFT ages were entered into HeFTy as constraints in T-t space that the cooling path must pass through, rather than input as thermochronologic ages. A closure temperature range of 240 ± ~15˚C (Bernet, 2009), which is characteristic of natural, radiation-damaged zircons at orogenic (~15 °C/Myr) cooling rates (e.g., Brandon et al., 1998), was used along with the age and error range of individual ZFT dates to define the area in T-t space that the cooling path had to pass through.

Inverse modeling for each sample used the following parameters: Search Method: "Monte Carlo" (default); Subsegment spacing: "Random" (default); Ending condition: "Paths tried = 10000" (default); Result to display: "Paths"; Weighted mean path function: "Nodal, GOF Product" (default); Merit value for 'good' fit: "0.5" (default); Merit value for 'acceptable fit' = "0.05" (default).

The HeFTy T-t paths from all eight samples are shown in Figure S8, with bounds of 275°C and 35 Ma. In the main text, the HeFTy paths are shown in Figure 8A-B, with bounds of 425°C and 75 Ma, in order to combine them with the higher-temperature T-t paths obtained from muscovite $^{40}Ar/^{39}Ar$ MDD modeling.

Figure S8 (following 2 pages). T-t paths for the Irwin Canyon granite samples, inverse-modeled in HeFTy.

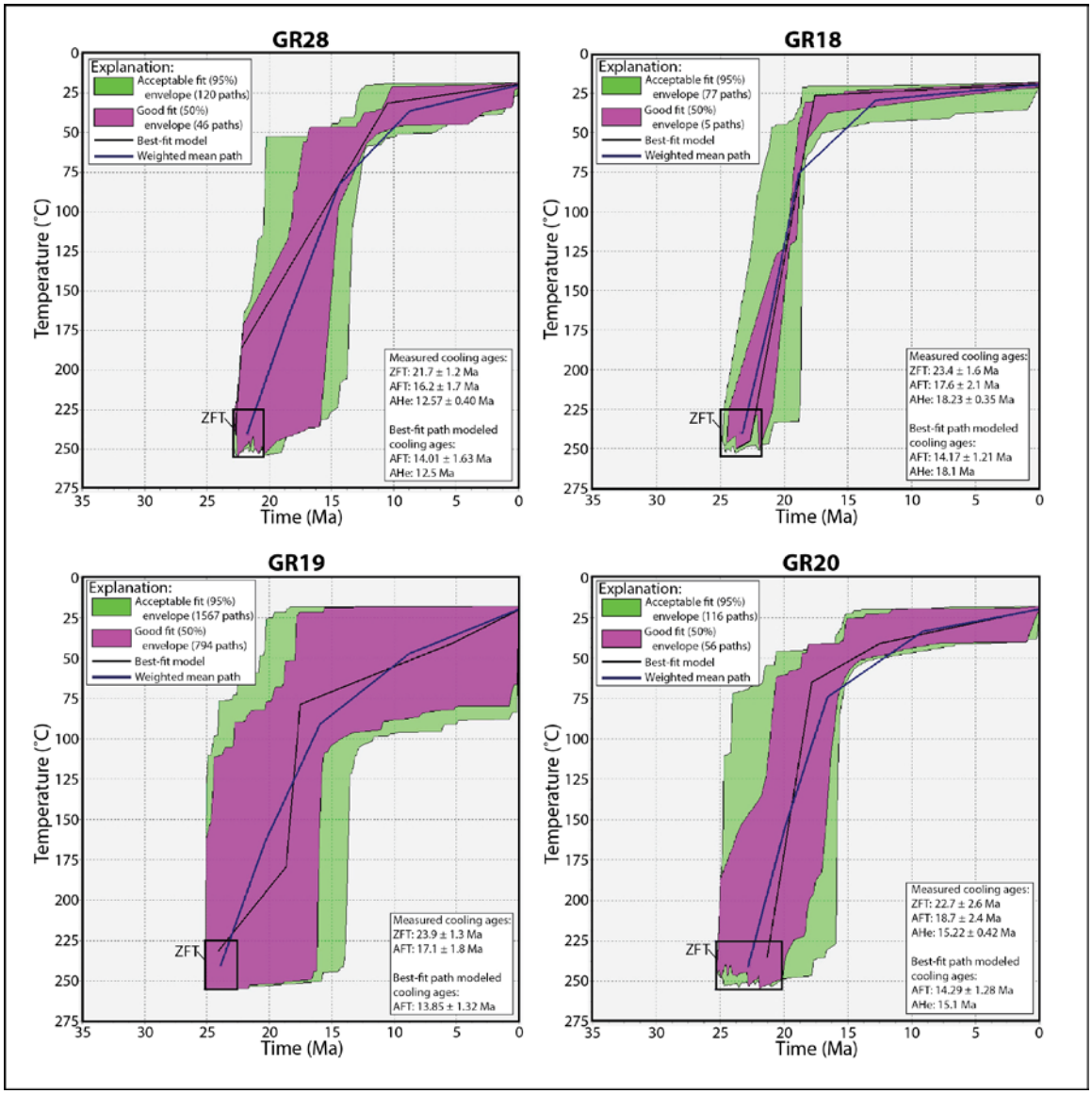
GR28
Explanation:
Acceptable fit (95%) envelope (120 paths)
Good fit (50%) envelope (46 paths)
Best-fit model
Weighted mean path
Measured cooling ages:
ZFT: 21.7 ± 1.2 Ma
AFT: 16.2 ± 1.7 Ma
AHe: 12.57 ± 0.40 Ma
Best-fit path modeled cooling ages:
AFT: 14.01 ± 1.63 Ma
AHe: 12.5 Ma
ZFT
Temperature (°C)
Time (Ma)
GR18
Explanation:
Acceptable fit (95%) envelope (77 paths)
Good fit (50%) envelope (5 paths)
Best-fit model
Weighted mean path
Measured cooling ages:
ZFT: 23.4 ± 1.6 Ma
AFT: 17.6 ± 2.1 Ma
AHe: 18.23 ± 0.35 Ma
Best-fit path modeled cooling ages:
AFT: 14.17 ± 1.21 Ma
AHe: 18.1 Ma
ZFT
Temperature (°C)
Time (Ma)
GR19
Explanation:
Acceptable fit (95%) envelope (1567 paths)
Good fit (50%) envelope (794 paths)
Best-fit model
Weighted mean path
Measured cooling ages:
ZFT: 23.9 ± 1.3 Ma
AFT: 17.1 ± 1.8 Ma
Best-fit path modeled cooling ages:
AFT: 13.85 ± 1.32 Ma
ZFT
Temperature (°C)
Time (Ma)
GR20
Explanation:
Acceptable fit (95%) envelope (116 paths)
Good fit (50%) envelope (56 paths)
Best-fit model
Weighted mean path
Measured cooling ages:
ZFT: 22.7 ± 2.6 Ma
AFT: 18.7 ± 2.4 Ma
AHe: 15.22 ± 0.42 Ma
Best-fit path modeled cooling ages:
AFT: 14.29 ± 1.28 Ma
AHe: 15.1 Ma
ZFT
Temperature (°C)
Time (Ma)

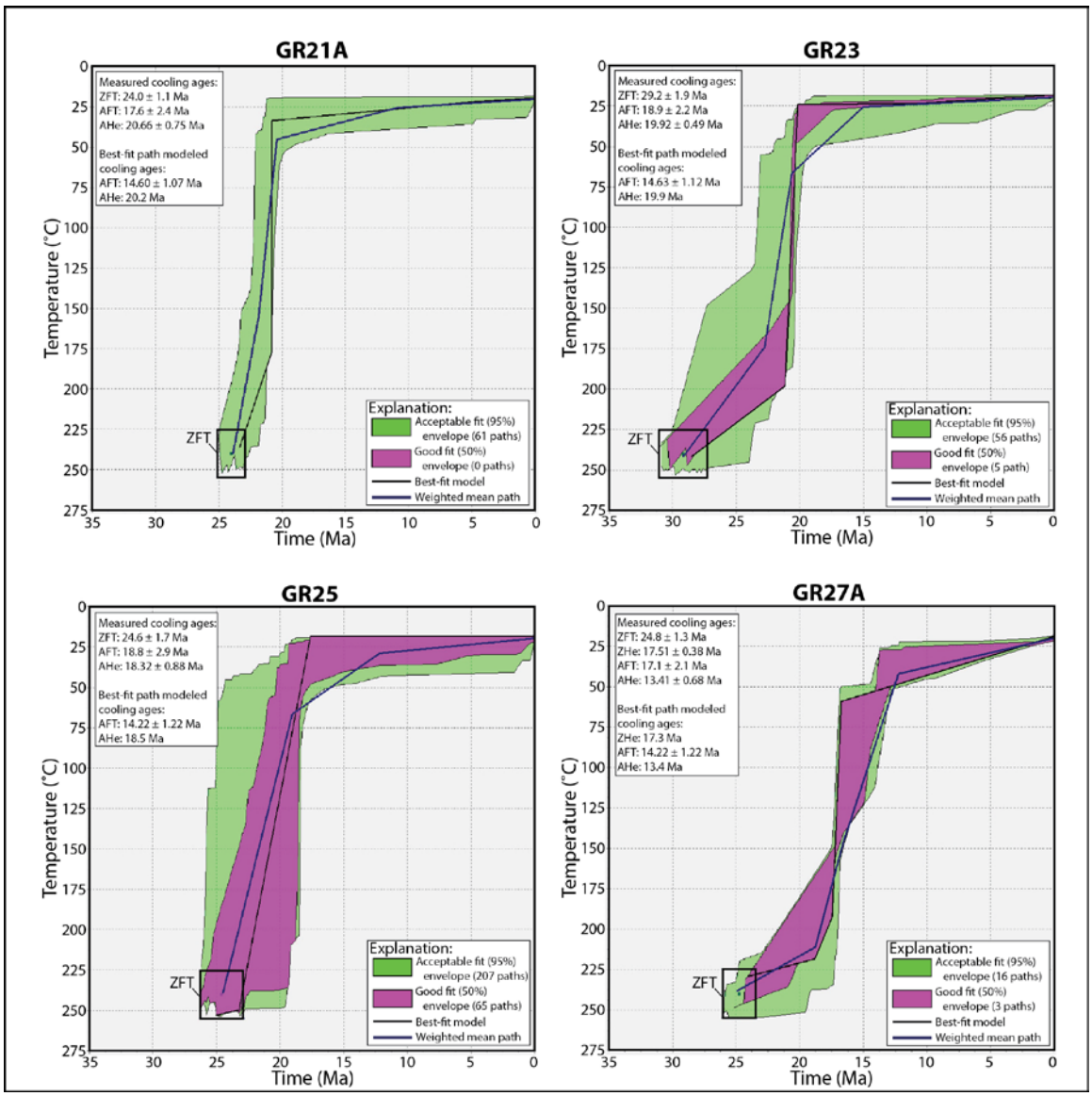

Text S12. Supporting information for 2-D kinematic forward modeling

Cross section A-A' was sequentially deformed and isostatically decompacted in six increments using Midland Valley Move version 2017.2 (results are shown on Figure 9 in the main text). First, an undeformed version of the cross section was drafted in Move. Motion on individual faults was performed using the '2D Move-on-Fault' module, using the 'Fault Parallel Flow' method, with the offset magnitude on each fault input from Table 1. After motion on a fault was performed, for each increment of deformation, isostatic rebound was then accounted for using the '2D Decompaction' module. The

following parameters were used: Main tab: 'Decompaction'; Bed Selection tab: Top Beds: the line representing the top of the Paleogene section from the previous deformation increment was selected here; Active Intermediate Objects: all lines on the cross section were selected here: Base: the line representing the top of the Paleogene section in the current deformation increment was selected here; Parameters tab: Get Parameters From: 'Default parameters'; Default Parameters: Initial Porosity '0.56 (default)'; Depth Coefficient: '0.39 km^{-1} (default)'; Grain Density: '2680 kg/m^3 (default)'; Compaction Curve: 'Sclater-Christie (default)'; Samples: '2000'; Trim Grid: '0'; Extend Grid: '3 (default)'; Filter Grid: '1 (default)'; Minimum Intersections: '3 (default)'; Decompact to: 'Use selected horizon (default)'. Isostatic Relief tab: Isostasy: 'Flex Isostasy'; Load: 'Sub Aerial Load'; Bulk Load Density: '2,600 kg/m^3'; Mantle Density: '3,300 km/m^3 (default)'; Elastic Thickness: '1,000 m (yielded a flexural wavelength of 33,088 m)'; Young's Modulus: '70,000 Mpa (default)'; Burial History tab: Selected Point X: '0.0 m (default)'. After motion on a fault, decompaction was then completed for that deformation increment. Then, the next youngest fault was drawn, slipped, and decompacted using a similar methodology.